Polymorphism and thermophysical properties of L- and DL-menthol

Vojtěch Štejfa [a,*], *Ala Bazyleva* [b], *Michal Fulem* [a], *Jan Rohlíček* [c], *Eliška Skořepová* [d], *Květoslav Růžička* [a], *Andrey V. Blokhin* [e]

[a] Department of Physical Chemistry, University of Chemistry and Technology, Prague, Technická 5, CZ-166 28 Prague 6, Czech Republic

[b] Applied Chemicals and Materials Division, National Institute of Standards and Technology, Boulder, CO 80305-3337, USA

[c] Institute of Physics of the Czech Academy of Sciences, Na Slovance 2, 182 21 Praha 8, Czech Republic

[d] Department of Chemical Engineering, University of Chemistry and Technology Prague, Technická 3, 16628, Prague 6, Czech Republic.

[e] Chemistry Faculty, Belarusian State University, Leningradskaya 14, 220030 Minsk, Belarus

*Corresponding author: stejfav@vscht.cz

This article is dedicated to the celebration of the contributions to Chemical Thermodynamics of Professor Gennady J. Kabo on the occasion of his 80th birthday.

Abstract

The thermodynamic properties, phase behaviour, and kinetics of polymorphic transformations of racemic (DL-) and enantiopure (L-) menthol were studied using a combination of advanced experimental techniques, including static vapour pressure measurements, adiabatic calorimetry, Tian-Calvet calorimetry, differential scanning calorimetry (DSC), and variable-temperature X-ray powder diffraction. Several concomitant polymorphs (α, β, γ, and δ forms) were observed and studied. A continuous transformation to the stable α form was detected by DSC and monitored in detail using X-ray powder diffraction. A long-term coexistence of the stable crystalline form with the liquid phase was observed. The vapour pressure measurements of both compounds were performed using two static apparatus over a temperature range from 274 K to 363 K. Condensed-phase heat capacities were measured by adiabatic and Tian-Calvet calorimetry in the wide temperature interval from 5 K to 368 K. Experimental data of L- and DL-menthol are compared mutually as well as with available literature results. The thermodynamic functions of crystalline and liquid L-menthol between 0 K and 370 K were calculated from the calorimetric results. The thermodynamic properties in the ideal-gas state were obtained by combining statistical thermodynamics and quantum chemical calculations based on a thorough conformational analysis. Calculated ideal-gas heat capacities and experimental data on vapour pressure and condensed-phase heat capacity were treated simultaneously to obtain a consistent thermodynamic description. Based on the obtained results, the phase diagrams of L-menthol and DL-menthol were suggested.

Keywords: monoterpenoids; menthol; vapour pressure; heat capacity; variable-temperature XRPD; thermodynamic properties; ideal gas; statistical thermodynamics.

1 Introduction

Menthol is a widely used chemical compound used in perfumes and cosmetics and serving as pharmaceutical excipient, food additive, and tobacco flavouring, due to its pleasant smell and cooling effect [1]. The compound is isolated as enantiopure L-menthol from natural peppermint oil or produced using either asymmetric synthesis or the Haarmann–Reimer process. In any of the production methods, isolation from multi-component systems via distillation, extraction, or crystallization is a necessary step. The recent increase of interest in the description of solid-liquid equilibria (SLE) [2-6] and liquid-liquid equilibria (LLE) [7] of menthol-based mixtures is likely related to an attempt to improve the process efficiency.

The four concomitant polymorphs of L-menthol and their transformations were described as early as 1917 [8], although the term “concomitant” for this uncommon behaviour itself was introduced much later [9]. Nowadays, both L- and DL-menthol are known to have several monotropically related polymorphs [2, 10, 11]. The crystal structures were solved for the α phase of both L-menthol [12] and DL-menthol [2], whereas only the cell parameters are known for the β polymorphs of L- and DL-menthol [2]. Neither crystallographic nor thermodynamic studies on the remaining known polymorphs (γ and δ phases of L-menthol and γ phase of DL-menthol, which were identified by visual observations, hot plate microscopy, and Flash DSC) have been conducted yet, except for enthalpy of fusion [10], because of their short lifetimes. Studies [11] and [2] traced interesting connections between polymorphism of enantiopure and racemic menthols and SLE behaviour of their mixture, and, although the conclusions are not in obvious agreement, some facts seem to be certain. Specifically, the α form of DL-menthol is a racemate (racemic compound) with low symmetry (space group $P\overline{1}$), whereas the β phase of DL-menthol is a pseudoracemate (solid solution), as evidenced by both X-ray and calorimetric studies. The β

polymorphs of L- and DL-menthol have very similar cell parameters and lack all but the periodic translational symmetry in the crystalline structure (space group *P*1). It should be noted that, inconsistently with the rest of the literature, Lipkind and Chickos [13] claimed that L-menthol exists in the form of a plastic crystal at room temperature. They supported the statement by a comment that it does not exhibit an X-ray diffraction pattern, which is contradicted by the pattern presented in [2].

Well defined thermodynamic properties and phase behaviour of a pure compound form a necessary basis for studies of related mixtures, especially in the case of complicated polymorphic behaviour, such as that of L- and DL-menthol. Considering the number of studies on menthol polymorphism and SLE behaviour of their mixtures, it is surprising, how little knowledge and agreement there is regarding thermodynamic properties of pure L- and DL-menthol. Temperatures and enthalpies of fusion of some polymorphs of L- and DL-menthol were reported several times, but a solid review and comparison of the previous values is needed. Heat capacities of the condensed phases for L-menthol were recently determined [6] by differential scanning calorimetry (DSC) which typically provides heat capacity data with much higher uncertainty than adiabatic or Tian-Calvet calorimetry. Vapour pressure measurements of menthols were performed in [14-17]. Only the data by Guetachew *et al.* [17] were measured by a direct method with a well-documented procedure giving the most reliable dataset for liquid L-menthol up to now.

In this work, a thorough study of thermodynamic properties and phase behaviour of L- and DL-menthol was carried out as a continuation of our effort [18-22] to establish reliable physico-chemical data for biogenic compounds relevant to environmental modelling as well as to other types of calculations and processes requiring phase equilibrium and thermodynamic data. The

experimental part consists of vapour pressure measurements using two static apparatus, and calorimetric measurements of the solid and liquid-phase heat capacities (adiabatic and Tian-Calvet calorimetry). Special attention was paid to obtaining the properties of all observed polymorphs and to guarantee the nature of the studied phases. To get a better insight into the phase transformations, DSC and variable-temperature X-ray powder diffraction (XRPD) were further used to investigate the phase behaviour and kinetics of the transformation between the polymorphs.

Developing a consistent thermodynamic description of L- and DL-menthol simultaneously considering measured vapour pressures and related thermal properties [23] requires thermodynamic properties in the ideal-gas state. These were obtained in this work by combining quantum-chemical and statistical-thermodynamics calculations.

2 Experimental and theoretical section

2.1 Materials

The description of the samples used in this work, including their purity, methods of purification, and purity analysis, is given in Table 1. Two samples of L-menthol from different sources were used in this work. All studied samples were of commercial origin. The enantiomeric excess in L-menthol from Fluka is stated by the producer to be 0.994, giving specific rotation of $[\alpha]_D^{20}$ = -50.3 degree·mL·g^{-1}·dm^{-1} (according to the supplier certificate). The enantiomeric composition in the natural L-menthol sample from RUE Belpharmatsiya was not separately determined, but it is expected to be comparable, according to the specific rotation of (-49 ± 1) degree·ml·g^{-1}·dm^{-1} (measured in an ATAGO automatic polarimeter AP-300 at T = 298.3 K and λ = 589 nm;

consistent with [12]). Handling of the samples prior to experiments was carried out under a dry nitrogen atmosphere in a glove box. The water content could not be measured for L-menthol from Fluka due to the small amount of the dry sample, but it is expected to be similar to that of DL-menthol. The water content in the L-menthol sample from RUE Belpharmatsiya was not separately determined, since the fractional-melting analysis applied to that sample is sensitive to all impurities, including water.

It should be emphasized that the purity was also checked after the measurements of vapour pressure and heat capacity using the Tian-Calvet calorimeter, and no decomposition was detected. The mole-fraction purity increased after the vapour pressure measurements to >0.9995 and 0.995 for L-menthol and DL-menthol, respectively, due to distilling off volatile impurities.

The atomic masses of elements recommended by IUPAC (conventional weights reported in Table 3 in [24]) were used to derive the molar mass of menthol: 0.156269 $kg \cdot mol^{-1}$, formula $C_{10}H_{20}O$.

Table 1

Sample description

Chemical name	CAS RN	Source	Mole fraction purity	Mass-fraction water content
Natural L-Menthol [a]	2216-51-5	RUE Belpharmatsiya	0.9973 [b]	N/A
L-Menthol [c]	2216-51-5	Fluka	0.999 [d]; 0.999 [e]	N/A
DL-Menthol [c]	89-78-1	SIAL	0.988 [d]; 0.992 [e]	$9 \cdot 10^{-6}$ [f]

[a] Sample used for the measurements by adiabatic calorimetry. The sample is a pharmaceutical ingredient. The sample was stored in a desiccator over P_2O_5 for a month prior to the experiments.

[b] Purity determined by fractional melting in an adiabatic calorimeter (see Table S1 and Figure S3 in the Supplementary Data (SD)). In addition, no impurity peaks were detected by gas chromatography using chromatograph HP 5890 Series II (equipped with a fused-silica capillary column coated with 0.25 μm HP-INNOWAX, 50 m length and 0.32 mm diameter, column temperature programmed between 323 K and 498 K) and HP 5972 quadrupole mass-selective detector (operated at 553 K).

[c] Samples used for the XRPD, vapour pressure, Tian-Calvet calorimetry, and DSC experiments. The samples were melted and dried over 0.4 nm molecular sieves (Merck).
[d] Purity provided by the manufacturer in the certificate of analysis determined by gas-liquid chromatography (GLC).
[e] Purity determined by GLC using the chromatograph Hewlett-Packard 6890A equipped with a column HP-1, length 25 m, film thickness 0.52 µm, diameter 0.30 mm, and FID detector in the temperature range from 313 to 523 K with inlet temperature of 373 K. Average of two determinations.
[f] Mass fraction of water determined by Karl-Fischer analysis by Metrohm 831. Average of three determinations.

2.2 Phase behaviour measurements

All temperatures reported in this paper are based on the international temperature scale ITS-90. The phase behaviour of the studied compounds was investigated from 273 K with a heat-flux differential scanning calorimeter TA Q1000 (TA Instruments, USA) using the continuous method with a heating rate of 2 $K \cdot min^{-1}$. The calorimeter was periodically calibrated with onset temperatures and enthalpies of fusion of five reference materials [25] selected to uniformly cover the desired temperature range: water (distilled and de-mineralized by Millipore RQ), gallium, naphthalene, indium, and tin (from the calibration set provided by GEFTA). The sample load of 5 mg to 10 mg was determined by an analytical balance that had resolution of 0.01 mg and was periodically calibrated.

2.3 X-ray powder diffraction experiments

To gain deeper insight into the solid phase transformations and behaviour of DL-menthol, variable temperature X-ray powder diffraction (VT-XRPD) was employed. The isothermal phase stability in the temperature range between 233 K and 303 K was studied by the XRPD technique using a powder diffractometer, Empyrean of PANalytical, which was equipped with a sealed Cu X-ray tube, capillary holder, PIXCel^{3D} detector, and an Oxford Cryostream cooling head. The sample was placed into several borosilicate capillaries with diameters of 0.5 mm and 0.7 mm. Two different techniques were used to fill the capillaries: (i) solid powder was ground at room

158 temperature and placed into a capillary, and (ii) a sample was melted and poured into the
159 capillary.
160 Two polymorphs (α and β) of DL-menthol were observed by XRPD, while γ has a too short
161 lifetime. The crystal structure of the stable α phase is known from single-crystal X-ray diffraction
162 [2]. Since the crystal structure of the metastable β phase is unknown, the Rietveld method [26]
163 could not be used to obtain the relative amount of the α and β phases in the samples. The
164 composition of the samples was instead determined from the change of the integrated intensities
165 of selected reflections during the measurement. In the case of the α phase, the ($\bar{1}$ 0 1) reflection
166 was used, and the peak corresponding to (2 1 0) and (2 $\bar{1}$ 0) reflections was used in the case of
167 the β phase. The approximate amount of the amorphous/liquid phase at 303 K was obtained
168 according to the principles published by Scarlett and Madsen [27].

169 *2.4 Heat capacity measurements by adiabatic calorimetry*

170 Heat capacities at the saturated vapour pressure ($C_{s,m}$) for the α-crystalline and liquid L-menthol
171 over the temperature range 5 K to 370 K and its melting parameters were measured in two
172 adiabatic calorimeters. The $C_{s,m}$ measurements between 5 K and 108 K (liquid-helium bath) were
173 conducted in a vacuum adiabatic calorimeter TAU-1 (VNIIFTRI, Moscow, Russia) described in
174 [28, 29]. The reliability of the heat-capacity measurements with the TAU-1 calorimeter was
175 verified in experiments with benzoic acid and high-purity copper, and the expanded uncertainty
176 with 0.95 level of confidence was estimated to be 2 % near 5 K and 0.4 % above 40 K [30]. A
177 vacuum adiabatic calorimeter TAU-10 (“Termis”, Moscow, Russia) was used between 80 K and
178 370 K (liquid-nitrogen bath) with the reproducibility and relative expanded uncertainty (0.95
179 level of confidence) of the $C_{s,m}$ measurements determined to be 0.1 % and 0.4 %, respectively.
180 The TAU-10 calorimeter details and verification experiments were described previously in [31].

During the experiments in both calorimeters, the temperature was measured with Fe-Rh resistance thermometers calibrated on ITS-90 at VNIIFTRI (Mendeleyevo, Moscow Region, Russia) with the standard uncertainty of 0.01 K.

Calorimetric cells made of stainless steel ($V \approx 1.0$ cm^3) in TAU-1 and of titanium ($V = 1.13$ cm^3) in TAU-10 were loaded with solid samples of 0.83748 g and 0.71244 g, respectively. The masses were determined with an accuracy of ±0.02 mg and corrected for buoyancy. After loading, the containers were degassed under vacuum (residual pressure of ~10 Pa) for 0.5 h. Helium gas ($p \approx 5$ kPa and $T = 293$ K) was introduced into the cell to facilitate heat transfer during the measurements. The containers were sealed using indium rings. The ratio of the sample heat capacity to the total (sample + cell) heat capacity was not less than 0.5 below 45 K and above the melting temperature and not less than 0.35 in between. The heat capacity of helium gas sealed in the calorimetric cell was accounted for in the treatment of the experimental data.

The temperature steps for the heat-capacity measurements were approximately equal to T/20 at $T < 40$ K and (1.5 to 2.5) K above 40 K. Heating periods were (80 to 150) s below 30 K, (200 to 300) s for T = (30 to 55) K, 380 s for T = (55 to 108) K in TAU-1, and 400 s in TAU-10. The thermal relaxation time was (80 to 200) s at $T < 60$ K, 230 s in TAU-1, and 150 s in TAU-10 at higher temperatures. The periods for the temperature-drift measurements were (70 to 200) s for $T < 60$ K, (200 to 250) s for T = (60 to 108) K in TAU-1, and (300 to 400) s in TAU-10. To obtain the sample purity and triple-point temperature, two fractional-melting experiments were conducted. The enthalpy of fusion was obtained from a combination of a series of experiments with continuous energy input (*i.e.*, one-step heating of the sample from a temperature below the beginning of the phase transition region to a temperature above it) and the two fractional-melting experiments.

Based on the vapour pressure of the sample measured in this work, an adjustment of $C_{s,m}$ to $C^0_{p,m}$ was much smaller than the experimental uncertainty in the studied temperature range and was neglected (*i.e.*, $C_{s,m} \approx C^0_{p,m}$).

2.5 Heat capacity measurements by Tian-Calvet calorimetry

Crystalline and liquid heat capacities of both L- and DL-menthol were also measured with a Tian-Calvet calorimeter (SETARAM μDSC IIIa, France) in the temperature range from 260 K to 359 K using the continuous method [32], whose performance was tested by Štejfa *et al.* [20]. A heating rate of 0.3 $K \cdot min^{-1}$ was used with isothermal delays of 2600 s before and after the continuous heating. After applying the standard procedures, including slope correction and signal smoothing, the heat capacity was calculated from the heat-flow record corresponding to an empty sample cell, the sample cell filled with synthetic sapphire (reference compound, NIST SRM 720), and subsequently with the sample. Approximately 10000 experimental heat capacity data points were obtained. For tabulation of the heat capacities obtained using the continuous method, the raw heat capacity data were averaged over 5 K intervals. The heat capacities are reported at the mean temperature of each 5 K interval. The combined expanded uncertainty (0.95 level of confidence) of the heat capacity measurements is estimated to be $U_c(C^0_{p,m}) = 0.01\ C^0_{p,m}$.

2.6 Vapour pressure measurements

Vapour pressure measurements were performed using the static method (with capacitance diaphragm gauges) with the STAT6 and STAT8 apparatus. The STAT6 and STAT8 apparatus were previously described in detail in [33] and [34], respectively, and thus only a concise description is provided here.

The performance of the STAT6 apparatus was checked by measurements of naphthalene, which is recommended for calibrating vapour pressure apparatus [35], and recently by *n*-octane and *n*-decane. The agreement with the recommended data [23, 35] was within the combined expanded uncertainty (0.95 level of confidence, k = 2) of the STAT6 apparatus, which is adequately described by $U_c(p/\mathrm{Pa}) = 0.005p/\mathrm{Pa} + 0.05$.

The STAT8 apparatus was calibrated by measurements of three reference materials, naphthalene, *n*-decane, and ferrocene, over the whole working range of the apparatus [34]. The combined expanded uncertainty of vapour pressure measurements $U_c(p)$ (0.95 level of confidence, k = 2) using the STAT8 apparatus was estimated based on the deviations of experimental data points from the recommended vapour pressures [23, 35, 36] to be $U_c(p/\mathrm{Pa}) = 0.01p/\mathrm{Pa} + 0.05$.

Prior to the measurement of the vapour pressure, both apparatus were checked for tightness by an MKS PICO helium leak detector (MKS Instruments, USA). The vapour pressure measurements were performed in the temperature interval from 274 K to 308 K and 277 K to 363 K with STAT6 and STAT8 apparatus, respectively, with *in situ* degassing of the sample through performing a large number of measuring cycles consisting of establishing the phase equilibrium followed by pumping of the vapour space formed. The measurements were carried out at selected temperatures repeated in a random order to track a systematic decrease of the measured pressure due to degassing of the sample. When that pressure decrease was negligible (after completing hundreds of measuring cycles enabled by full automation of the apparatus), the sample was considered completely degassed, and the final set of data was recorded. At least three experimental points were obtained for each temperature.

246 *2.7 Theoretical calculations*

247 The conformational study, optimization of molecular geometries, energy and harmonic frequency
248 calculations, and scans of potential energy of internal rotations were performed with the Gaussian
249 09 software [37] using the density functional theory (DFT) at the B3LYP-D3/6-311+G(d,p) level
250 of theory. The energies of the most stable (triequatorial) conformers were also recalculated using
251 LCCSD(T)/aug-cc-pVQZ with the MRCC software package [38] for structures optimized at the
252 DF-MP2/aug-cc-pVQZ level of theory with Psi4 v. 1.1 [39], where LCCSD(T) is an efficient
253 local coupled-cluster method proposed recently [40] and DF-MP2 is the Møller-Plesett second-
254 order perturbation theory in density-fitted (also referred to as "resolution-of-identity", RI)
255 approximation. The detailed conformational study was performed, as the number and relative
256 energies of conformers are crucial for calculating ideal-gas properties. After obtaining structures
257 for all stable conformers, the thermodynamic properties of enantiopure menthol in the ideal-gas
258 state were calculated by statistical thermodynamics using the R1SM model. This model combines
259 the RRHO ("rigid rotor–harmonic oscillator") approximation with a correction for methyl
260 rotations using the 1-D HR ("one-dimensional hindered rotor") formalism [41] for each
261 conformer and subsequent application of the mixing model [42]

262 $$C^0_{p,\mathrm{m}} = \sum_{i=1}^{N} x_i C^0_{p,\mathrm{m},i} + \frac{1}{RT^2} \sum_{i=1}^{N} x_i \sum_{j>i}^{N} x_j \left(\Delta_\mathrm{r} H_{ij}(0\,\mathrm{K})\right)^2 , \quad (1)$$

263 $$S^0_\mathrm{m} = \sum_{i=1}^{N} x_i S^0_{\mathrm{m},i} - R \sum_{i=1}^{N} x_i \ln x_i , \quad (2)$$

264 where x_i are the mole fractions of the corresponding conformers at temperature T,

265 $$x_i = e^{-\frac{\Delta G_i(T)}{RT}} \Big/ \sum_{j=1}^{N} e^{-\frac{\Delta G_j(T)}{RT}} , \quad (3)$$

N is the number of conformers (including their optical isomers for achiral molecules), $\Delta_r H_{ij}(0\,\mathrm{K})$ is the enthalpy of transformation of the i^{th} conformer to the j^{th} conformer at 0 K, $\Delta G_i(T)$ is the relative Gibbs energy of i-th conformer (designation "relative" means relative to the most stable conformer for all properties in Eqs. (3) and (4)), and $C^0_{p,\mathrm{m},i}$ and $S^0_{\mathrm{m},i}$ are the ideal-gas heat capacity and standard ideal-gas entropy of the i^{th} conformer. $\Delta G_i(T)$ is calculated as:

$$\Delta G_i(T) = \Delta E_i^{0\,\mathrm{K}} + \Delta E_i^{\mathrm{ZPE}} + \Delta H_i^{\mathrm{Therm}}(T) - T\Delta S_i(T), \quad (4)$$

where $\Delta S_i(T)$ is the relative entropy of i-th conformer, $\Delta H_i^{\mathrm{Therm}}(T)$ is the relative thermal enthalpy of i-th conformer, $\Delta E_i^{\mathrm{ZPE}}$ is the relative zero-point vibrational energy, and $\Delta E_i^{0\,\mathrm{K}}$ is the relative electronic energy. $\Delta S_i(T)$, $\Delta H_i^{\mathrm{Therm}}(T)$, and $\Delta E_i^{\mathrm{ZPE}}$ are calculated in the RRHO approximation with 1-D HR correction for the methyl tops. Similar approach was used in our previous works [21, 43, 44]. Relative electronic energies and zero-point vibrational energies of the conformers were included from the calculation at the B3LYP-D3/6-311+G(d,p) level of theory, except for the electronic energies of the most stable (triequatorial) conformers, which were calculated at the LCCSD(T)/aug-cc-pVQZ level of theory, as described above.

The B3LYP-D3/6-311+G(d,p) calculated fundamental frequencies were scaled by a double-linear scaling factor (0.9980 – 1.55E-05 ν/(cm^{-1})) / 0.961 for frequencies below/above 2000 cm^{-1} developed on experimental vibrational frequencies of *n*-alkanes. The contributions of internal rotations of methyl tops were calculated using the 1-D HR scheme, which required the energy barriers and the reduced moments of inertia I_r for methyl rotations, the internal symmetry number (σ_i = 3), and the identification and exclusion of these torsional modes from the vibrational contribution to the partition function. The potential energy profiles of methyl rotations were

calculated at the B3LYP-D3/6-311+G(d,p) level of theory using a relaxed scan with a step of 10° for the most stable conformer. The reduced moments of inertia I_r for methyl rotations were calculated according to Pitzer and Gwinn [45] from the optimized molecular parameters. The energy levels were obtained by solving a one-dimensional Schrödinger equation for hindered internal rotation using the FGH method [46].

3 Results and discussion

3.1 Phase behaviour

In this work, we focused on the characterization of the polymorphs of L- and DL-menthol by thermodynamic and diffraction techniques. Not all of the described polymorphs of these compounds can be studied by these techniques. The stability and/or preparation conditions of the metastable forms limit their study significantly, since common techniques, such as adiabatic calorimetry, Tian-Calvet calorimetry, or static measurements of the vapour pressure, are too slow. We were able to detect melting of the α, β, γ and δ polymorphs of L-menthol and of the α and β polymorphs of DL-menthol using DSC, although Corvis *et al.* [10] suggested that the γ form of L-menthol can be detected only when using flash DSC. On the other hand, the γ phase of DL-menthol observed in [10] was not detected in this work.

Several modifications of L-menthol seem to crystalize simultaneously and immediately start to transform to more stable modifications when running DSC experiments. Such behaviour, denoted as concomitant polymorphism, is rare but documented for some other compounds [9]. The first task was an accurate measurement of fusion enthalpy of the α polymorph ($\Delta^{l}_{\alpha}H^{0}_{m}$) using DSC, since the results varied even in experiments, where a single peak was detected in the thermogram. Therefore, the α phases of both L- and DL-menthol were prepared in the DSC by two

approaches: (i) heating a crystallized sample slightly above the β phase melting temperature ($T_{\mathrm{fus},\beta}$) followed by cooling well below it, and (ii) long isothermal conversion from the β phase at temperatures around 273 K or 293 K for DL- and L-menthol, respectively. It should be noted that the spontaneous phase change from the β to α phase is not accompanied by any exothermal effect within the detection limits of the TA Q1000 calorimeter at given conditions. The DSC runs with the α phase prepared by melting of the β phase usually yielded a single peak at the melting temperature corresponding to the α phase ($T_{\mathrm{fus},\alpha}$). However, $\Delta^{\mathrm{l}}_{\alpha}H^{0}_{\mathrm{m}}$ of both DL- and L-menthol obtained by this process are (0.5 to 1) kJ mol^{-1} lower than that for the α polymorph prepared by transformation of the β phase, although there were no signs of any other peak in the DSC thermogram, except for a few experiments with DL-menthol performed at a high heating rate, where a subtle peak of melting of the β phase was observed (in agreement with XPRD observation in Figure S4 in SD). The resulting assumption that the subcooled liquid phase may coexist with the α phase for a long time period was further studied using XRPD and examined during adiabatic measurements. The transformation and crystallization rate of the α phase was also observed to be lower for L-menthol than for DL-menthol.

Even though several combinations of heating rates and quenching times were tested, it was not possible to obtain the fusion enthalpy of the metastable forms of L-menthol directly. The melting enthalpy of the β polymorph ($\Delta^{\mathrm{l}}_{\beta}H^{0}_{\mathrm{m}}$) was calculated from the DSC runs where the melting peaks of the α and β phases were of comparable size. The ratio of polymorphs was derived from the $\Delta^{\mathrm{l}}_{\alpha}H^{0}_{\mathrm{m}}$ of the pure α phase, *i.e.*, as $\Delta^{\mathrm{l}}_{\beta}H^{0}_{\mathrm{m}} = A_{\beta}\Big/\left(1 - A_{\alpha}/\Delta^{\mathrm{l}}_{\alpha}H^{0}_{\mathrm{m}}\right)$, where A is the melting peak area per chemical amount of the whole sample. The melting enthalpies of the γ and δ polymorphs of L-menthol have higher uncertainty as they were calculated from experiments with three or four

partially overlapping melting peaks, as shown in Figure 1. Separation of the peaks using a lower heating rate is not possible due to the short lifetime of the metastable polymorphs since their melt immediately crystallizes to more stable phases. Several different thermograms are displayed in Figure 1 together with a demonstration of the $\Delta^{l}_{\beta}H^{0}_{\mathrm{m}}$ calculation. The measurements for DL-menthol showed certain differences relative to L-menthol. Quenching of the melt to 288 K followed by fast heating, suggested in [2], resulted in a direct measurement of $\Delta^{l}_{\beta}H^{0}_{\mathrm{m}}$ of DL-menthol. The resulting value was in excellent agreement with a value calculated following the methodology for L-menthol. Any other polymorphs of DL-menthol were not detected. The fusion temperatures and enthalpies of all observed polymorphs of L-and DL-menthol are listed in Table 2.

To obtain reliable condensed-phase properties (heat capacity and melting parameters) of the stable α phase of L-menthol, adiabatic calorimetry was used. Since adiabatic calorimetry measurements are very slow by their nature (each heat-capacity point takes 15 min to 30 min on average) and rapid cooling is not achievable (typical cooling rate is around 0.03 $\mathrm{K \cdot s^{-1}}$ around room temperature), all regular procedures by the method gave only the stable α phase of L-menthol without any traces of metastable modifications. In addition, crystals were annealed at ~298 K for (4-5) hours in the adiabatic calorimeter to make sure that no metastable modification remained. In all adiabatic calorimetry series, reproducible enthalpy of fusion of the α phase was observed (see Table S2 in the SD for details).

We were also able to determine heat capacity and vapour pressure of the β phase of DL-menthol during experiments using the Tian-Calvet calorimeter and STAT6. The same was not possible

during measurements for L-menthol nor using STAT8 apparatus due to its slower cooling rate compared to STAT6.

The literature values for normal $T_{fus,\alpha}$ of L-menthol range from 315 K to 316.7 K. Three values obtained in this work by different techniques (DSC, adiabatic calorimetry, and vapour pressure measurements) for two independent samples fit within the range from 315.4 K to 315.6 K and lie in the lower part of the interval. On the other hand, $T_{fus,\beta}$ = 310.0 K measured in this work for L-menthol is higher than most of the literature values ranging from 308.5 K to 310.7 K. The explanation of this slight disagreement in not evident as purity, enantiomeric excess in the sample, or calibration of DSC should not significantly affect the difference between the melting points of polymorphs. Values of $\Delta^{l}_{\alpha}H^{0}_{m}$ summarized in Table 2 exhibit a scatter larger than 2 kJ·mol^{-1}, which could be probably assigned to the observed long-term coexistence of the α form and liquid. Most of the values (including the difference in slope of our vapour pressure measurements and excepting for the value reported in [2]) are about 0.5 kJ·mol^{-1} lower than our DSC and adiabatic results, corresponding rather to our DSC experiments performed with the samples containing the residual liquid (see the pink thermogram in Figure 1). XRPD results for DL-menthol also support a long-term co-existence of the liquid and α form as discussed in the next section. However, we note that the phase change mechanisms may be different for L- and DL-menthol and affected by different experimental conditions including container materials and sample mass. The data on $\Delta^{l}_{cr}H^{0}_{m}$ and T_{fus} of other L-menthol polymorphs are scarce, however, the values are in reasonable agreement considering the difficulties associated with their determinations.

Only two records on $\Delta^{l}_{cr}H^{0}_{m}$ and T_{fus} for the α and β polymorphs of DL-menthol were found in the literature, [2] (both polymorphs) and [47] (one polymorph). From the comparison of the results, it is obvious that $\Delta^{l}_{\beta}H^{0}_{m}$ and $T_{fus,\beta}$ are reported in [47] although the polymorphism is not mentioned in the paper and the study itself focused on differences in properties of pure enantiomers and racemic crystals (note that β-DL-menthol is a pseudoracemate). There is a slight disagreement in the value of $\Delta^{l}_{\alpha}H^{0}_{m}$ and $T_{fus,\alpha}$ measured in this work and in [2], similarly to L-menthol. Our result obtained by DSC is in close agreement with that obtained using the vapour pressure measurements and, therefore, seems to be more reliable. On the other hand, $\Delta^{l}_{\beta}H^{0}_{m}$ and $T_{fus,\beta}$ of DL-menthol from all sources are in a good agreement.

The melting properties of menthols were previously studied mostly by DSC, so all the available data summarized in Table 2 should have comparable uncertainties, while the new data from adiabatic calorimetry for the α polymorph of L-menthol have uncertainties lower by a factor of ten. The reported uncertainties of some literature values in Table 2 can be considered too optimistic, if inherent uncertainties of the DSC method and complicated phase behaviour of menthol are taken into account. We recommend the adiabatic calorimetry results for the α form of L-menthol and mean values of the DSC and vapour pressure results in the other cases (given as bold values in Table 2). The use of the melting parameters for the α form of L-menthol from adiabatic calorimetry is justified, since (i) weighted mean of the available values would yield an almost identical value due to the large difference in realistically estimated uncertainties, (ii) the enthalpies of fusion from the literature can be subject to the presence of residual liquid, as discussed above, and (iii) when deriving the thermodynamic functions from the heat capacity and

melting parameters in Section 3.3, the use of consistent total enthalpies upon integration is required.

Table 2

Temperatures and enthalpies of fusion of L- and DL-menthol at 0.1 MPa.[a]

polymorph	L-menthol		DL-menthol	
	T_{fus} / K	$\Delta^{l}_{cr}H^{0}_{m}$ / kJ mol^{-1}	T_{fus} / K	$\Delta^{l}_{cr}H^{0}_{m}$ / kJ mol^{-1}
α phase	**315.60 ± 0.02** [b,c] 315.4 ± 0.3 [d] 315.4 [e] 316.1 ± 0.3 [2] 316 [f] [47] 316.7 ± 0.1 [3] 315 [48] 315.6 [8] 315.7 [11] 315.4 [49] 315.6 [50]	**13.47 ± 0.06** [b,c] 13.3 ± 0.3 [d] 12.5 [e] 14.1 ± 0.2 [2] 11.9 [f] [47] 12.83 ± 0.10 [3] 12.4 [48]	305.7 ± 0.3 [d] 305.9 [e] 307.0 ± 0.3 [2] 307.2 [11] **306.5 ± 0.8 (mean)** [c]	13.7 ± 0.3 [d] 13.7 [e] 14.2 ± 0.2 [2] **13.9 ± 0.3 (mean)** [c]
β phase	310.0 ± 0.3 [d] 308.5 ± 0.3 [2] 308.6 [8] 310.7 [11] 309.5 [50] **309.5 ± 0.9 (mean)** [c]	11.4± 0.5 [d] 11.0 ± 0.2 [2] **11.2 ± 0.3 (mean)** [c]	300.7 ± 0.4 [d] 300.5 [e] 300.5 ± 0.3 [2] 301 [f] [47] 300.5 [11] **300.6 ± 0.1 (mean)** [c]	9.9 ± 0.4 [d] 10.0 [e] 9.3 ± 0.2 [2] 10.3 [f] [47] **9.7 ± 0.4 (mean)** [c]
γ phase	308.7 ± 0.5 [d,g] 306.0 ± 0.6 [10] 306.6 [8] 309.7 [11] **307.8 ± 1.7 (mean)** [c]	6.7 ± 2.0 [d,g] 6.2 [10] **6.5 ± 0.4 (mean)** [c]	295.9 ± 0.6 [10] 296.5 [2] [h]	1.9 ± 0.2 [10]
δ phase	304.3 ± 1.0 [d,g] 304.6 [8] 306.2 [11] **305.0 ± 1.0 (mean)** [c]	7.3 ± 2.0 [d,g]		

[a] Only literature values obtained during calorimetric studies (DSC, if not specified otherwise) and vapour pressure studies are included. The type of uncertainty for the literature values was not specified in the corresponding sources except for [3], where the uncertainty is described as standard uncertainty.

[b] This work, triple-point temperature from adiabatic calorimetry. Expanded uncertainties with 0.95 level of confidence are provided.

[c] Recommended value (in bold) calculated either as average of DSC results (specified uncertainty is the expanded uncertainties with 0.95 level of confidence) or as an adiabatic-calorimetry value when available.

[d] This work, DSC TA Q1000. Expanded uncertainties with 0.95 level of confidence are provided.

[e] This work, calculated from the vapour pressure measurements using static method (STAT6 and STAT8 apparatus). The value of $\Delta_{cr}^{l} H_{m}^{0}$ for L-menthol is affected by the coexistence of the α phase and liquid.

[f] Measured by DTA without specification of the corresponding polymorph. We matched the data to specific phases according to the specified T_{fus}.

[g] The γ- and δ-phase melting peaks are always followed by crystallization or overlap with melting of more stable polymorphs (see Figure 1). The determination of T_{fus} and $\Delta_{cr}^{l} H_{m}^{0}$ for these forms is therefore less accurate.

[h] Indirect determination from Roozeboom's melting loop.

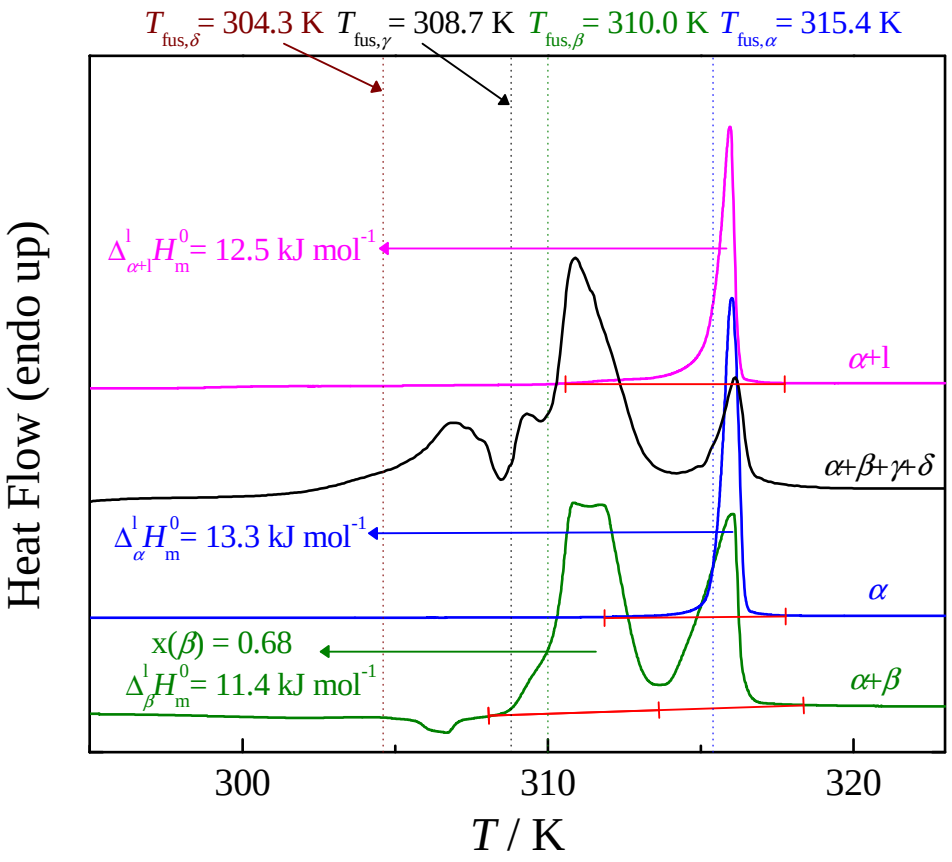

Figure 1. Phase behaviour of L-menthol at 0.1 MPa. Thermograms were recorded in the heating mode with different heating rates (HR), scaled and shifted for clarity. —, HR = 2 K·min^{-1}, freshly crystallized sample, demonstration of calculation of $\Delta_{\beta}^{l} H_{m}^{0}$; —, HR = 0.5 K·min^{-1}, the aged α sample obtained by

transformation from the β-phase; ━, HR = 10 K·min^{-1}, freshly crystallized sample; ━, HR = 2 K·min^{-1}, the α sample prepared by crystallization followed by heating to 313 K (above $T_{fus,\beta}$).

3.2 X-ray study and kinetics of transformation of DL-menthol from the β to α phase

The maximum lifetime of β-DL-menthol was observed to be tens of minutes up to several hours depending on the maintained temperature in both vapour pressure and DSC measurements. The VT-XRPD method was also employed since it enables *in-situ* monitoring of the polymorphic composition. A series of XRPD measurements was performed to determine isothermal conversion rate of the β to α polymorph at various temperatures. DL-menthol was selected for the study, as the occurrence of the other polymorphs of L-menthol would complicate the study. However, the transformation of the β to α polymorph in the case of L-menthol is believed to behave in a qualitatively similar way, although it was observed to be slower during the DSC experiments.

The phase conversion curves were recorded at several temperatures between 233 K and 298 K and fitted by the Johnson-Mehl-Avrami (JMA) equation [51]:

$$x(\beta) = e^{-k(t-t_0)^n}, \quad (5)$$

where $x(\beta)$ is the fraction of the β polymorph, t_0 is the initial lag (induction time) before the phase change started, n is a geometric parameter determining the nature of nucleation, and k is the rate constant of the transformation. The induction time of a (re)crystallization process has a stochastic nature. Therefore, as expected, the t_0 value was found to be highly variable during the experiments at the same temperature and acted primarily for aligning the curves during the treatment. The fitting procedure was found to be only weakly dependent on n, which varied between 1.5 and 3 for different curves. Finally, $n = 2$ was fixed, which would, from theory,

443 correspond to the heterogeneous nucleation and crystal growth in one dimension [51], which
444 matches well with the needle shape of menthol crystals.
445 The smoothed conversion curves and the temperature dependence of the parameter k and phase
446 change half-life $\tau_{1/2}$ are displayed in Figure 2. The obtained parameters of the conversion curves
447 with respect to temperature are listed in Table S3 in the SD. Our results demonstrate that the β-α
448 phase transition proceeds continuously with the highest transformation rate around 268 K as a
449 result of interplay between thermodynamic and kinetic aspects. These conclusions are in
450 agreement with a previous stability study [2], although we did not detect any decrease of the β-
451 phase stability above 288 K.
452 Another XRPD experiment was designed to support the assumption of coexistence of the super
453 cooled liquid and the α phase. A liquid DL-menthol sample was quenched to 288 K and left to
454 crystallize, thereby initiating a continuous transformation from β to α. When reaching $x(\beta) \approx 0.8$,
455 the sample was heated to 303 K with the heating rate of about 4 $K \cdot min^{-1}$, where the β phase
456 melted. The gradual increase in the intensity of the α-phase reflections and the decrease in the
457 background halo demonstrated in Figure S5 in the SI proved the coexistence of the liquid and α
458 phase on the order of hours, although the assessment has a large uncertainty. The measurements
459 indicate there is a residual (and not detectably decreasing) ratio of amorphous phase in DL-
460 menthol even after 24 hours at 303 K. Even after a repeated cooling, the liquid part of the sample
461 coexisting with the α phase was observed to crystallize into the β phase by both DSC and XRPD,
462 which, however, transformed to the α phase in a relatively short time (see Figure S4 in the SI).
463 Considering the slow α-phase formation from both the liquid and β phase, the rate-determining
464 step is probably the organization of the molecules into the α-phase lattice. The comparison of the

experiments in Figure 3 also suggests that the rate of formation of the α phase by transformation from the β phase is faster than by crystallization from the liquid phase.

It should be also noted that we have performed a successful indexation of the β phase of DL-menthol with the resulting unit cell identical to the one reported in [2]. The complicated nature of the crystal structure, however, did not allow for the full structure solution from the XRPD data. This understanding of the phase behaviour and kinetics of transformations between various menthol polymorphs provided a necessary foundation for the systematic study of thermodynamic properties of menthols described in the following sections.

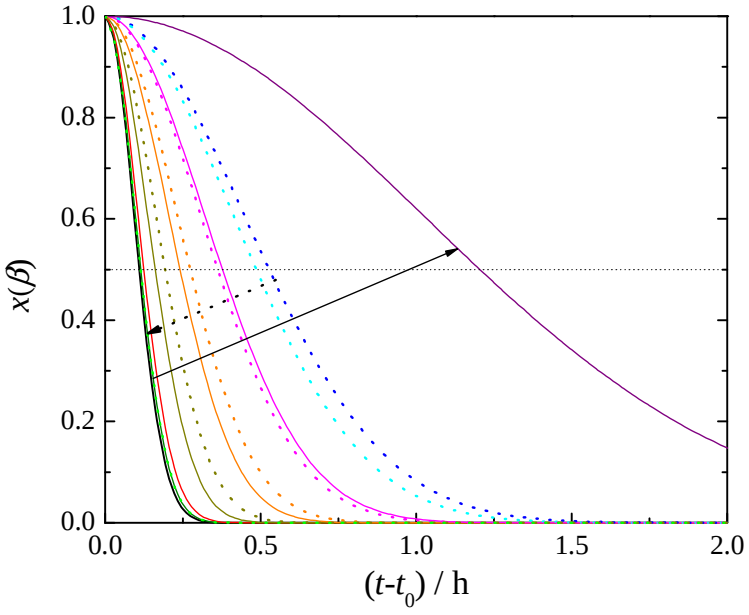

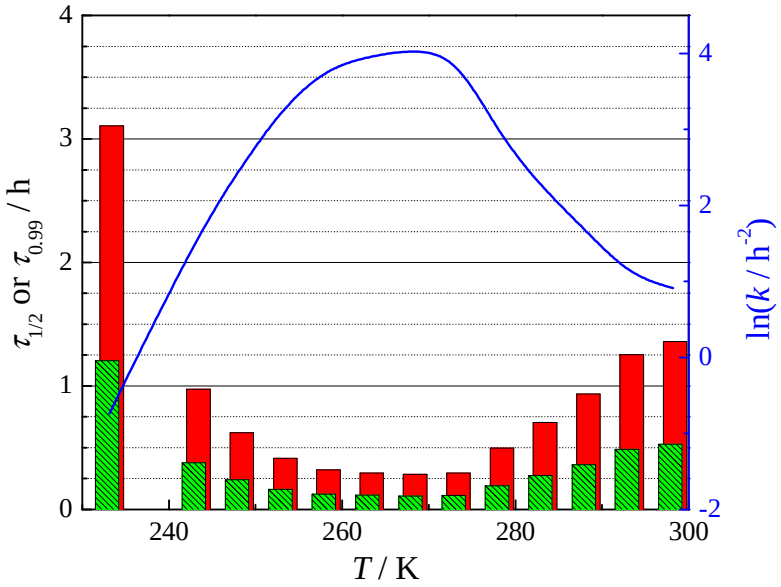

Figure 2. Conversion of the β to α phase of DL-menthol at different temperatures.

Top: $x(\beta)$ is the fraction of the β polymorph. JMA kinetics curves are shown instead of experimental points for clarity. Temperature of annealing: ┈┈, 298 K; ┈┈, 293 K; ┈┈, 288 K; ┈┈, 283 K; ┈┈, 278 K; ┈┈, 273 K; ━, 268 K (change of trend); ━, 263 K; ━, 258 K; ━, 253 K; ━, 248 K; ━, 243 K; ━, 233 K; Bottom: Kinetics parameters: ━, rate constant k from Eq. (5) (right axis), ▮ (hatched), phase change half-life, $\tau_{1/2}$; ▮, phase change 99th percentile, $\tau_{0.99}$ (left axis).

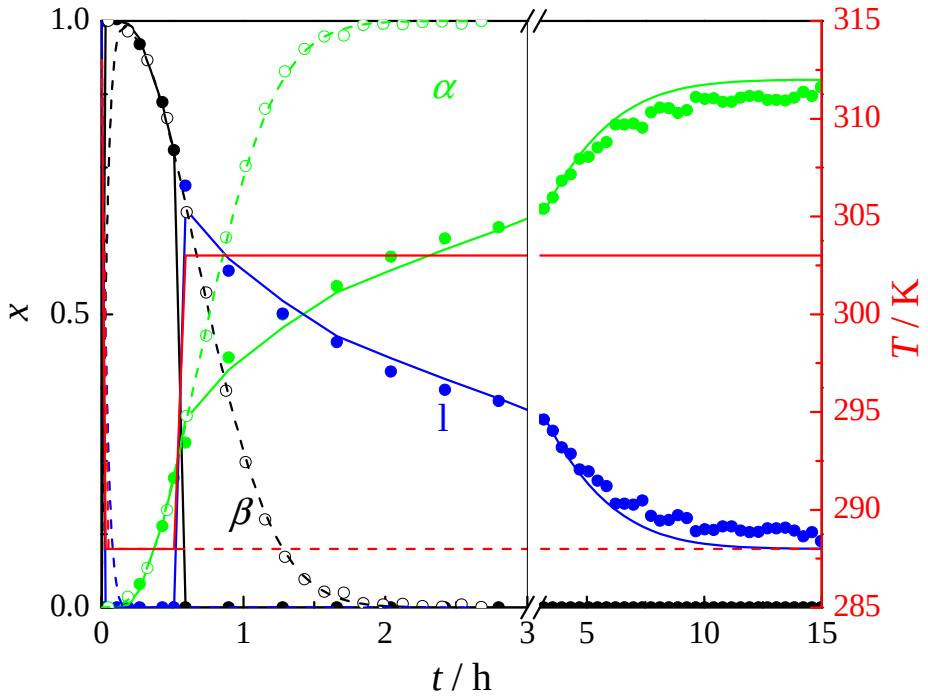

Figure 3. Comparison of kinetics of formation of the α phase by crystallization and by phase transformation from the β phase for DL-menthol.

—, temperature (right axis); —,●, $x = x(\mathrm{l})$; —,●, $x = x(\alpha)$; —,●, $x = x(\beta)$. Lines are calculated from the JMA equation, Eq. (5). Full symbols and solid lines belong to measurement at 303 K (above $T_{\mathrm{fus},\beta}$), empty symbols and dashed lines to measurement at 288 K (below $T_{\mathrm{fus},\beta}$).

3.3 Condensed phase heat capacities

The experimental molar heat capacities of the α phase and liquid L-menthol measured in the adiabatic calorimeter are presented in Table 3 and shown graphically in Figure 4. The experimental heat capacities of the α-crystalline and liquid phase of L- and DL-menthols obtained by Tian-Calvet calorimetry are listed in Table 4 and displayed in Figure 5. The latter measurements of the α phase were performed after maintaining the sample at 273 K for 3 hours which was estimated as a sufficient time for a complete transformation as confirmed by the absence of a β-phase melting peak. Since it was possible to obtain the pure β form of DL-menthol

498 in the DSC, measurements by Tian-Calvet calorimetry were repeated with a freshly crystallized
499 sample and resulted in noticeably lower heat capacities which were assigned to the β polymorph
500 with a possible small amount of the α phase that may have been formed during the course of the
501 experiment.
502 As it is obvious from Table 4 and Figure 5, the heat capacities of both α-crystalline and liquid L-
503 menthol obtained from two independent methods in this work are consistent within the
504 uncertainty of a heat capacity determination by Tian-Calvet calorimetry, with the exception of the
505 heat capacity data of the α form obtained by Tian-Calvet calorimetry above 280 K. These data are
506 slightly higher due to that fact that they were not corrected for the premelting effects and a
507 possibly higher water content of the sample used. The effect of water contamination is within the
508 claimed uncertainty for the liquid phase, and the agreement of the results for L-menthol can serve
509 as a validation for the results obtained with the Tian-Calvet calorimeter for DL-menthol. The heat
510 capacities of the liquid L- and DL-samples are equal to within their experimental uncertainties,
511 but for the α phases, the heat capacity of DL-menthol is provably lower over the studied
512 temperature range by about 1 % to 2 %.
513 The heat capacities of liquid and α-crystalline L-menthol from Corvis and Espeau [6] are in a
514 remarkably good agreement with our results (within 3 %) when considering that a heat-flux DSC
515 was employed. It should be noted that the authors of [6] used a three-run procedure, repeated the
516 experiments several times with different samples and obtained deviations from reference data for
517 testing compounds (water and naphthalene) up to 10 %. By comparing with the reference data, a
518 steeper slope of temperature dependence of heat capacity data reported in [6] can be seen. The
519 authors claimed a somewhat optimistic expanded uncertainty (0.95 level of confidence) for L-
520 menthol (1.2 % to 3.2 %, which most likely reflects only a statistical component of uncertainty,

i.e., type A uncertainty) when compared to the uncertainties of their measurements with the reference materials. Corvis and Espeau [6] also reported heat capacities of the β for of L-menthol between 204 K and 226 K, which are 11 % to 16 % lower than our adiabatic calorimetry results for the α polymorph of L-menthol. A lower heat capacity for the metastable phase is in agreement with our results on DL-menthol, but such a large difference between the two polymorphs is unlikely.

To maintain internal consistency of the condensed-phase thermodynamic data, the heat-capacity and melting-parameter data for L-menthol from the adiabatic calorimetry were used in further calculations. The lower uncertainty of adiabatic calorimetry in comparison with Tian-Calvet calorimetry and DSC also justified the choice. In deriving the thermodynamic functions of L-menthol in the condensed state from (5 to 370) K, smoothing of heat capacities above 5 K was carried out with the use of overlapping polynomials. Heat capacities below 5 K were extrapolated with a Debye function with three degrees of freedom: $C^0_{p,\mathrm{m}} = 3R \cdot D(\langle\Theta_\mathrm{D}\rangle / T)$, where the average Debye characteristic temperature was derived to be $\langle\Theta_\mathrm{D}\rangle = 65.6$ K from the experimental heat capacities between (5.0 and 9.5) K. Table 5 summarizes the thermodynamic functions of L-menthol.

For user's convenience, the experimental data from Tian-Calvet calorimeter for DL-menthol were represented by a polynomial equation:

$$C^0_{p,\mathrm{m}} \Big/ \left(\mathrm{J\ K^{-1}\ mol^{-1}}\right) = a + b\left(\frac{T}{100\ \mathrm{K}}\right) + c\left(\frac{T}{100\ \mathrm{K}}\right)^2 \qquad (6)$$

with parameters given in Table 6. All measured data points obtained (not just the averaged values presented in Table 4) were used for deriving the polynomials.

Table 3

Experimental molar saturation-pressure heat capacities for L-menthol obtained by adiabatic calorimetry [a]

T / K	$C_{s,m}$ / J·K^{-1}·mol^{-1}
Series 1 (TAU-1)	
crystal (α phase)	
5.02	0.8545
5.31	1.027
5.63	1.231
5.95	1.445
6.26	1.675
6.62	1.937
7.00	2.276
7.37	2.577
7.74	2.937
8.14	3.382
8.58	3.847
9.03	4.373
9.49	4.870
9.99	5.512
10.51	6.205
11.04	6.889
11.61	7.681
12.20	8.523
12.83	9.473
13.48	10.42
14.15	11.42
14.89	12.53
15.66	13.66
16.43	14.93
17.26	16.13
18.12	17.43
19.04	18.89
20.00	20.23
21.02	21.71
22.08	23.27
23.20	24.92
24.41	26.58
25.66	28.24
26.93	29.92
28.27	31.55
29.67	33.28
31.12	34.98
32.66	36.66
34.28	38.41
36.00	40.06
37.89	42.03
39.90	43.93
42.02	45.96
44.24	48.03
46.54	50.11
48.92	52.21
51.35	54.32
53.83	56.47
56.32	58.63
58.78	60.81
61.29	62.85
64.03	65.18
66.85	67.74
69.53	70.14
72.08	72.41
74.60	74.48
77.11	76.77
79.66	78.77
82.26	80.88
84.79	83.06
87.34	85.27
89.90	87.37
92.42	89.76
94.94	91.69
97.47	93.81
100.02	95.95
102.58	98.22
105.18	100.4
107.78	102.4
Series 2 (TAU-10)	
crystal (α phase)	
79.78	79.07
81.50	80.47
83.22	81.89
84.94	83.28
86.67	84.77
88.39	86.22
90.12	87.73
91.85	89.21
93.59	90.65
95.32	92.09
97.06	93.51
98.80	95.01
100.55	96.44
102.30	97.81
104.04	99.24
105.80	100.7
107.55	102.0
109.31	103.5
111.06	104.9
112.82	106.2
114.58	107.7
116.34	109.0
118.11	110.4
119.87	111.7
121.64	113.1
123.41	114.4
125.18	115.8
126.95	117.2
128.73	118.4
130.50	119.8
132.28	121.1
134.07	122.4
135.85	123.7
137.63	125.1
139.41	126.4
141.20	127.7
142.99	128.9
144.77	130.2
146.56	131.5
148.36	132.8
150.15	134.1
151.94	135.3
153.73	136.6
155.53	137.9
157.32	139.1
159.12	140.4
160.91	141.7
162.72	143.0
164.52	144.3
166.32	145.5
168.12	146.8
169.92	148.0
171.73	149.2
173.53	150.5
175.33	151.8
177.14	153.1
178.95	154.4
180.76	155.6
182.56	156.9
184.37	158.2
186.18	159.4
188.00	160.7
189.81	162.1
191.62	163.3
193.43	164.6
195.25	165.9
197.06	167.2
198.87	168.5
200.69	169.8
202.50	171.1

T / K	$C_{s,m}$ / J·K^{-1}·mol^{-1}
204.32	172.4
206.14	173.7
207.95	175.0
209.77	176.4
211.60	177.6
213.42	178.9
215.24	180.2
217.07	181.5
218.89	182.9
220.72	184.2
222.55	185.4
Series 3 (TAU-10)	
crystal (α phase)	
216.36	180.9
218.32	182.5
220.14	183.7
221.96	185.1
223.78	186.5
225.60	187.8
227.43	189.1
229.25	190.5
231.07	191.9
232.89	193.3
234.71	194.7
236.53	196.1
238.35	197.4
240.18	198.8
242.00	200.2
243.83	201.7
245.65	203.1
247.48	204.5
249.30	206.0
251.12	207.5
252.95	208.9
254.77	210.4
256.59	212.0
258.41	213.7
260.23	215.2
262.05	216.8
263.88	218.5
265.70	220.1
267.52	221.7
269.34	223.4
271.17	225.1
272.99	226.5
274.82	227.9
276.64	229.6
278.46	231.1
280.29	232.6
282.11	234.2
283.93	235.8
285.75	237.3
287.57	239.0

T / K	$C_{s,m}$ / J·K^{-1}·mol^{-1}
289.39	240.8
291.22	242.6
293.04	244.4
294.86	246.6
296.68	248.4
298.50	250.6
300.32	252.8
302.14	255.3
303.96	258.2
305.78	261.9
307.59	267.2
309.39	276.9
311.16	301.9
312.80	399.7
314.05	917.0
314.83	3386
315.18	15063
315.34	39619
liquid	
317.43	826.2
321.01	384.9
323.45	388.5
325.28	391.1
327.12	393.8
328.95	396.4
330.79	399.1
332.62	401.7
334.46	404.2
336.30	406.5
338.14	408.8
339.98	411.3
341.82	413.4
343.66	415.8
345.50	417.9
347.35	419.8
349.19	421.7
351.04	423.4
352.88	425.1
354.73	426.7
356.58	428.4
358.43	429.7
360.27	431.1
362.12	432.6
363.97	433.8
365.82	435.5
367.67	436.2
Series 4 (TAU-10)	
crystal (α phase)	
278.81	231.4
280.63	233.0
282.45	234.5
284.26	236.1
286.08	237.7

T / K	$C_{s,m}$ / J·K^{-1}·mol^{-1}
287.88	239.5
289.68	241.3
291.47	242.9
293.25	244.8
295.02	246.7
296.79	248.6
298.55	250.5
300.30	252.7
302.05	255.2
303.78	257.9
305.50	261.4
307.21	266.1
308.90	274.2
310.55	291.8
312.60	435.0
314.23	1451
314.88	4980
315.12	10054
315.24	16051
315.32	24245
315.37	38440
315.41	68331
liquid	
316.10	1070
318.10	380.3
320.34	383.5
322.18	386.6
324.01	389.3
325.85	392.2
327.67	394.8
329.49	397.5
331.30	400.1
333.11	402.5
Series 5 (TAU-10)	
liquid, including super cooled liquid	
312.20	370.6
314.15	373.6
316.02	376.5
317.87	379.7
319.72	382.6
321.56	385.4
323.40	388.2
Series 6 (TAU-10)	
crystal (α phase)	
290.89	242.4
292.76	244.5
294.53	246.2
continuous energy input	
306.62	874.7
liquid	
318.47	380.7

T / K	$C_{s,m}$ / J·K^{-1}·mol^{-1}
Series 7 (TAU-10)	
crystal (α phase)	
291.80	243.3
293.66	245.4
295.44	247.2
continuous energy input	
307.48	880.9
liquid	
319.28	381.8
Series 8 (TAU-10)	
crystal (α phase)	
291.08	242.5
293.06	244.7
294.94	246.6
296.82	248.6
298.69	250.9
300.55	252.9
302.40	255.6
304.24	258.6
306.07	262.6
307.88	268.6
309.65	279.9
311.85	350.8
313.82	896.7
314.72	3282
315.03	7459
315.19	12074
315.28	18701
315.34	27475
315.39	42162
315.42	63161
liquid	
316.21	819.2
317.57	379.5
318.82	381.4
320.06	383.3
321.31	385.3
322.55	386.9
323.79	388.8
Series 9 (TAU-10)	
liquid	
320.78	384.6
323.31	388.4
325.83	392.0
328.34	395.8
330.84	399.3
333.33	402.6
335.81	406.0
338.29	409.0
340.77	412.1
343.25	415.1
345.72	418.1
348.20	420.7
350.66	423.0
353.12	425.1
355.58	427.2
358.04	429.4
360.49	431.0
362.94	432.8
365.39	434.2
367.84	435.7

[a] Average heat capacities at the mean temperatures of experiments. The measurements were performed at p(He) = (5 ± 1) kPa (the pressure value corresponds to T = 293 K); no adjustment of $C_{s,m}$ to $C^0_{p,m}$ at $p^0 = 10^5$ Pa (*i.e.*, $C_{s,m} \approx C^0_{p,m}$) is needed due to small vapour pressure of the sample. The expanded uncertainty is $U(T)$ = 0.02 K, the relative expanded uncertainties are $U_r(C_{s,m}) = 0.02 - 4.57\cdot10^{-4}((T / \mathrm{K}) - 5)$ at 5 K < T < 40 K and $U_r(C_{s,m}) = 0.004$ at T > 40 K for 0.95 level of confidence (k = 2).

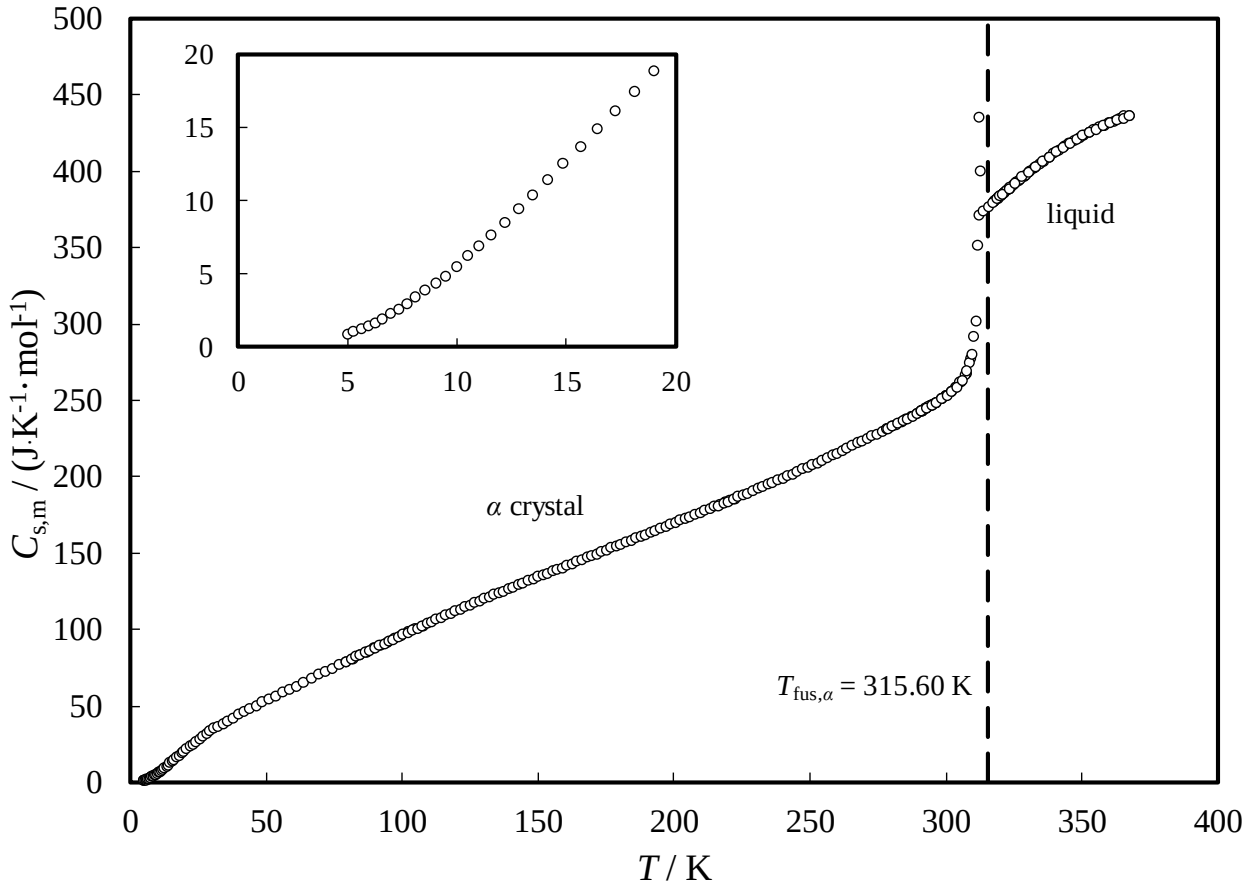

Figure 4. Condensed-phase heat capacities of L-menthol from adiabatic calorimetry measurements

Table 4

Experimental standard molar heat capacities of the condensed phases $C^0_{p,m}$ measured by the Tian-Calvet calorimeter at 100 kPa. [a]

T / K	$C^0_{p,m}$ / J K^{-1} mol^{-1}	$\Delta C^0_{p,m}$ [b]	T / K	$C^0_{p,m}$ / J K^{-1} mol^{-1}	$\Delta C^0_{p,m}$ [b]
L-Menthol m = 0.59114 g			DL-Menthol m = 0.52334 g		
α-crystalline			α-crystalline		
265.2	221.5	0.79%	265.0	217.6	-0.01%
270.0	225.6	0.78%	270.0	221.3	0.03%
275.0	230.0	0.82%	275.0	225.3	0.04%
280.0	235.1	1.19%	280.0	229.5	-0.03%
285.0	240.5	1.58%	285.0	234.2	0.00%
290.0	246.3	1.99%			
295.0	253.1	2.63%			

	liquid			liquid	
325.9	395.1	0.74%	315.4	377.3	0.06%
330.0	401.1	0.75%	320.0	384.2	-0.10%
335.0	408.0	0.75%	325.0	392.0	-0.07%
340.0	414.3	0.73%	330.0	399.8	0.07%
345.0	420.5	0.82%	335.0	406.9	0.13%
350.0	426.2	0.90%	340.0	412.7	0.01%
355.0	430.8	0.89%	345.0	418.1	-0.11%
			350.0	423.7	-0.06%
			355.0	429.0	0.03%
			β-crystalline		
			270.0	217.5	0.15%
			275.0	219.5	0.07%
			280.0	223.1	-0.07%
			285.0	229.0	0.05%

[a] The standard uncertainty of the temperature is $u(T) = 0.05$ K, and the combined expanded uncertainty of the heat capacity is $U_c(C^0_{p,m}) = 0.01\,C^0_{p,m}$ (0.95 level of confidence). Mean values of four determinations.

[b] $\Delta C^0_{p,m} = 100 \cdot \left(C^0_{p,m} - C^{0,calc}_{p,m}\right) \Big/ C^{0,calc}_{p,m}$ is the relative deviation from the fit; $C^{0,calc}_{p,m}$ was taken from Table 5 and calculated using Eq. (6) with parameters listed in Table 6 for L- and DL-menthol, respectively.

Table 5

Standard molar thermodynamic functions of L-menthol in the crystalline and liquid states at a standard pressure of 100 kPa [a]

T / K	$C^0_{p,\mathrm{m}}$	$\Delta_0^T H^0_\mathrm{m} / T$	$\Delta_0^T S^0_\mathrm{m}$	$-\Delta_0^T G^0_\mathrm{m} / T$
	$\mathrm{J{\cdot}K^{-1}{\cdot}mol^{-1}}$			
Crystal (α phase)				
5	0.858 ± 0.017	0.2148 ± 0.0043	0.2864 ± 0.0057	0.0716 ± 0.0014
10	5.528 ± 0.098	1.548 ± 0.029	2.099 ± 0.040	0.552 ± 0.010
15	12.70 ± 0.20	4.037 ± 0.069	5.656 ± 0.098	1.619 ± 0.028
20	20.26 ± 0.27	7.15 ± 0.11	10.35 ± 0.17	3.198 ± 0.050
25	27.36 ± 0.30	10.49 ± 0.15	15.64 ± 0.23	5.151 ± 0.073
30	33.65 ± 0.29	13.84 ± 0.17	21.20 ± 0.28	7.362 ± 0.094
35	39.12 ± 0.25	17.07 ± 0.18	26.81 ± 0.32	9.74 ± 0.11
40	44.06 ± 0.18	20.14 ± 0.19	32.36 ± 0.35	12.22 ± 0.12
45	48.69 ± 0.19	23.06 ± 0.19	37.82 ± 0.37	14.76 ± 0.13
50	53.14 ± 0.21	25.84 ± 0.19	43.18 ± 0.40	17.34 ± 0.14
55	57.47 ± 0.23	28.52 ± 0.19	48.45 ± 0.42	19.93 ± 0.15
60	61.81 ± 0.25	31.12 ± 0.20	53.64 ± 0.44	22.52 ± 0.16
65	66.15 ± 0.26	33.64 ± 0.20	58.76 ± 0.46	25.11 ± 0.17
70	70.48 ± 0.28	36.12 ± 0.21	63.82 ± 0.48	27.70 ± 0.18
75	74.81 ± 0.30	38.56 ± 0.21	68.83 ± 0.50	30.27 ± 0.19
80	79.11 ± 0.32	40.96 ± 0.22	73.79 ± 0.52	32.84 ± 0.20
85	83.38 ± 0.33	43.33 ± 0.22	78.72 ± 0.54	35.39 ± 0.21
90	87.62 ± 0.35	45.67 ± 0.23	83.60 ± 0.56	37.93 ± 0.22
95	91.81 ± 0.37	47.99 ± 0.24	88.45 ± 0.58	40.47 ± 0.23
100	95.95 ± 0.38	50.28 ± 0.24	93.27 ± 0.60	42.98 ± 0.24
105	100.0 ± 0.4	52.55 ± 0.25	98.05 ± 0.62	45.49 ± 0.25
110	104.0 ± 0.4	54.80 ± 0.26	102.8 ± 0.6	47.99 ± 0.26
115	108.0 ± 0.4	57.03 ± 0.27	107.5 ± 0.7	50.48 ± 0.27
120	111.8 ± 0.4	59.24 ± 0.27	112.2 ± 0.7	52.95 ± 0.28
125	115.7 ± 0.5	61.42 ± 0.28	116.8 ± 0.7	55.41 ± 0.29
130	119.4 ± 0.5	63.57 ± 0.29	121.4 ± 0.7	57.86 ± 0.30
135	123.1 ± 0.5	65.71 ± 0.29	126.0 ± 0.7	60.30 ± 0.31
140	126.8 ± 0.5	67.83 ± 0.30	130.6 ± 0.7	62.73 ± 0.32
145	130.4 ± 0.5	69.92 ± 0.31	135.1 ± 0.8	65.15 ± 0.33
150	134.0 ± 0.5	72.00 ± 0.32	139.5 ± 0.8	67.55 ± 0.34
155	137.5 ± 0.6	74.05 ± 0.32	144.0 ± 0.8	69.95 ± 0.35
160	141.1 ± 0.6	76.09 ± 0.33	148.4 ± 0.8	72.33 ± 0.36
165	144.6 ± 0.6	78.11 ± 0.34	152.8 ± 0.8	74.70 ± 0.37
170	148.1 ± 0.6	80.12 ± 0.35	157.2 ± 0.9	77.06 ± 0.38
175	151.6 ± 0.6	82.11 ± 0.35	161.5 ± 0.9	79.42 ± 0.38
180	155.1 ± 0.6	84.09 ± 0.36	165.8 ± 0.9	81.76 ± 0.39
185	158.6 ± 0.6	86.06 ± 0.37	170.1 ± 0.9	84.09 ± 0.40
190	162.2 ± 0.6	88.01 ± 0.37	174.4 ± 0.9	86.41 ± 0.41
195	165.7 ± 0.7	89.96 ± 0.38	178.7 ± 0.9	88.72 ± 0.42
200	169.3 ± 0.7	91.90 ± 0.39	182.9 ± 1.0	91.02 ± 0.43
205	172.8 ± 0.7	93.83 ± 0.40	187.1 ± 1.0	93.31 ± 0.44
210	176.4 ± 0.7	95.75 ± 0.40	191.4 ± 1.0	95.60 ± 0.45
215	180.0 ± 0.7	97.67 ± 0.41	195.5 ± 1.0	97.87 ± 0.46

T / K	$C^0_{p,\mathrm{m}}$	$\Delta_0^T H^0_\mathrm{m} / T$	$\Delta_0^T S^0_\mathrm{m}$	$-\Delta_0^T G^0_\mathrm{m} / T$
	$J \cdot K^{-1} \cdot mol^{-1}$			
220	183.7 ± 0.7	99.59 ± 0.42	199.7 ± 1.0	100.1 ± 0.5
225	187.4 ± 0.7	101.5 ± 0.4	203.9 ± 1.0	102.4 ± 0.5
230	191.1 ± 0.8	103.4 ± 0.4	208.1 ± 1.1	104.7 ± 0.5
235	194.9 ± 0.8	105.3 ± 0.4	212.2 ± 1.1	106.9 ± 0.5
240	198.7 ± 0.8	107.2 ± 0.4	216.3 ± 1.1	109.1 ± 0.5
245	202.5 ± 0.8	109.1 ± 0.5	220.5 ± 1.1	111.4 ± 0.5
250	206.5 ± 0.8	111.0 ± 0.5	224.6 ± 1.1	113.6 ± 0.5
255	210.7 ± 0.8	112.9 ± 0.5	228.7 ± 1.1	115.8 ± 0.5
260	215.1 ± 0.9	114.9 ± 0.5	232.9 ± 1.2	118.0 ± 0.5
265	219.5 ± 0.9	116.8 ± 0.5	237.0 ± 1.2	120.2 ± 0.5
270	223.9 ± 0.9	118.7 ± 0.5	241.2 ± 1.2	122.4 ± 0.6
275	228.2 ± 0.9	120.7 ± 0.5	245.3 ± 1.2	124.6 ± 0.6
280	232.4 ± 0.9	122.6 ± 0.5	249.5 ± 1.2	126.8 ± 0.6
285	236.7 ± 0.9	124.6 ± 0.5	253.6 ± 1.2	129.0 ± 0.6
290	241.5 ± 1.0	126.6 ± 0.5	257.8 ± 1.3	131.2 ± 0.6
295	246.7 ± 1.0	128.6 ± 0.5	261.9 ± 1.3	133.4 ± 0.6
298.15	250.1 ± 1.0	129.8 ± 0.5	264.6 ± 1.3	134.7 ± 0.6
300	252.3 ± 1.0	130.6 ± 0.5	266.1 ± 1.3	135.5 ± 0.6
305	258.3 ± 1.0	132.6 ± 0.5	270.4 ± 1.3	137.7 ± 0.6
310	264.6 ± 1.1	134.7 ± 0.6	274.6 ± 1.3	139.9 ± 0.6
315	271.4 ± 1.1	136.8 ± 0.6	278.9 ± 1.3	142.1 ± 0.6
315.60	272.3 ± 1.1	137.1 ± 0.6	279.4 ± 1.3	142.3 ± 0.6
Liquid				
315.60	376.1 ± 1.5	179.8 ± 0.7	322.1 ± 1.5	142.3 ± 0.6
320	383.1 ± 1.5	182.5 ± 0.7	327.3 ± 1.5	144.8 ± 0.6
325	390.8 ± 1.6	185.7 ± 0.8	333.3 ± 1.6	147.7 ± 0.6
330	398.1 ± 1.6	188.8 ± 0.8	339.4 ± 1.6	150.5 ± 0.7
335	404.9 ± 1.6	192.0 ± 0.8	345.4 ± 1.6	153.4 ± 0.7
340	411.3 ± 1.6	195.2 ± 0.8	351.5 ± 1.6	156.3 ± 0.7
345	417.1 ± 1.7	198.4 ± 0.8	357.5 ± 1.7	159.2 ± 0.7
350	422.3 ± 1.7	201.5 ± 0.8	363.5 ± 1.7	162.0 ± 0.7
355	427.0 ± 1.7	204.7 ± 0.8	369.6 ± 1.7	164.9 ± 0.7
360	431.0 ± 1.7	207.8 ± 0.8	375.6 ± 1.7	167.8 ± 0.7
365	434.3 ± 1.7	210.9 ± 0.9	381.5 ± 1.8	170.7 ± 0.7
370	437.0 ± 1.7	213.9 ± 0.9	387.5 ± 1.8	173.6 ± 0.8

[a] Expanded uncertainties with 0.95 confidence level are reported.

Table 6

Parameters of Eq. (6) for $C^0_{p,\mathrm{m}}$ and standard deviation of the fit σ.

compound	a	b	c	$(T_{\min} - T_{\max})$[a] / K	σ_r [b]
DL-menthol (α crystal)	553.04	-321.48	73.550	262 – 291	0.04
DL-menthol (β crystal)	2646.2	-1826.2	343.17	265 – 288	0.18
DL-menthol (liquid)	-1070.81	750.86	-92.51	313 – 359	0.10

[a] Temperature range of experimental points used for development of the polynomial. We only present polynomials for measurements by Tian-Calvet calorimetry, while smoothed data are listed for adiabatic measurements in Table 4.

[b] $\sigma_r = 100\left[\sum_{i=1}^{n}\left(C^0_{p,\mathrm{m}}/C^{0,\mathrm{calc}}_{p,\mathrm{m}} - 1\right)_i^2 \Big/ (n-m)\right]^{1/2}$, where n is the number of fitted data points and m is the number of adjustable parameters.

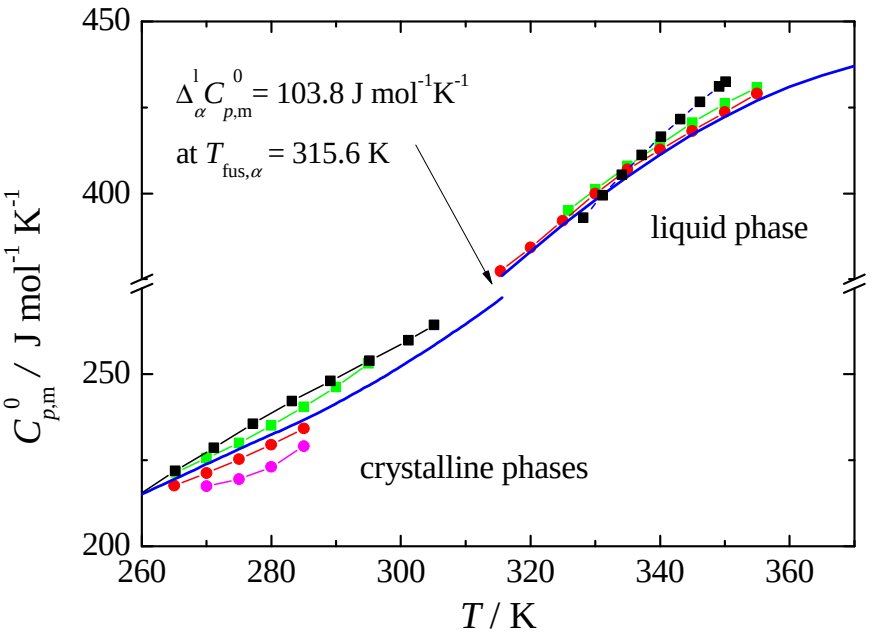

Figure 5. Condensed phase heat capacities $C^0_{p,\mathrm{m}}$. L-menthol (α crystal and liquid): —, adiabatic calorimetry (smoothed data visualized for clarity); ■, Tian-Calvet calorimetry; ■, Corvis *et al.*, DSC [6]; DL-menthol: ●, Tian-Calvet calorimetry (α crystal and liquid); ●, Tian-Calvet calorimetry (β crystal). Note the break on the *y*-axis between the crystalline phases and liquid phases.

3.4 Vapour pressures

The vapour pressures of liquid and α-crystalline menthols were measured using two static apparatus. The temporary stability of β-DL-menthol (on the order of tens of minutes) enabled measurements of its vapour pressures using STAT6, however with a higher uncertainty. In this case, the first measurement after crystallization had to be considered, which shows a slightly effect from insufficient stabilization of temperature. Still, the measurements can definitely be assigned to the β phase, as demonstrated in Figure 6, and they are in good agreement with other thermodynamically linked data. The lifetime of the other metastable polymorphs is much shorter than the time scale of the vapour pressure measurements, which typically take days or weeks.

The vapour pressures determined in this work are listed in Table 7 and Table 8. The vapour pressure data determined using both apparatus for the same phases agree within the experimental uncertainties as displayed in Figure 7. A multi-phase arc plot representation was used to visualize the vapour pressure data as the common view ($\ln p$ as a function of $1/T$) does not provide reasonable resolution between the phases and between individual experimental points. The construction of such a multi-phase arc plot (described in [52] and reprinted in the SD for reader's convenience) is based on arc representation [53], but it allows visualization of vapour pressure data of multiple condensed phases.

The vapour pressure measurements for the liquid and α phase of L-menthol are not consistent with $\Delta^{\mathrm{l}}_{\alpha}H^{0}_{\mathrm{m}}$ obtained by DSC and adiabatic calorimetry, but rather with a value obtained during DSC experiments with a residual fraction of liquid. We assume that even during the vapour pressure measurements, the L-menthol sample did not completely crystallize to the α-form despite one week of continuous measurement below $T_{\mathrm{fus},\alpha}$ (after a degassing procedure in the

liquid phase). The crystallization in the static apparatus always took place during isotherms between 301 K and 303 K, where crystallization of the β phase probably could not occur and the slow direct crystallization of the α phase could result in a residual coexistence with the liquid. Since kinetics of the transformation as well as the diffusion between the phases may affect the measured pressure, no correction to obtain the sublimation pressure of the α phase was attempted. The correlation for the α form of L-menthol was developed based on the liquid vapour pressures, fusion properties, and heat capacities measured by adiabatic calorimetry.

Table 7

Experimental vapour pressures measured using STAT6 apparatus. [a]

T / K	p / Pa [b]	Δp/Pa [c]	T / K	p / Pa [b]	Δp/Pa [c]
L-menthol			DL-menthol		
α-Crystalline + liquid phase [d]			*α-Crystalline phase*		
273.64	0.244	0.014	273.65	0.259	0.001
273.65	0.244	0.013	273.65	0.259	0.001
273.65	0.242	0.011	273.66	0.261	0.003
278.15	0.441	0.019	278.16	0.480	0.004
278.15	0.440	0.018	278.16	0.479	0.003
278.16	0.440	0.017	278.16	0.477	0.001
283.15	0.839	0.032	283.15	0.922	0.006
283.15	0.839	0.033	283.16	0.921	0.004
283.15	0.840	0.034	283.16	0.926	0.009
288.15	1.559	0.053	288.16	1.736	0.009
288.15	1.557	0.051	288.16	1.734	0.007
288.16	1.558	0.050	288.16	1.734	0.007
293.14	2.829	0.082	293.14	3.173	0.001
293.14	2.828	0.080	293.14	3.180	0.008
293.14	2.831	0.083	293.15	3.183	0.007
298.15	5.047	0.127	298.16	5.734	0.002
298.15	5.039	0.119	298.16	5.733	0.001
298.15	5.033	0.113	298.16	5.730	-0.002
303.14	8.771	0.157	303.14	10.09	-0.01
303.14	8.757	0.143	303.14	10.10	0.00
303.14	8.761	0.147	303.15	10.10	-0.02
308.15	15.01	0.18	*Liquid phase*		
308.15	15.00	0.17	293.14	3.971	0.005
308.15	15.00	0.17	293.14	3.966	0.000
Liquid phase			293.14	3.969	0.003
308.15	16.72	-0.01	298.13	6.551	0.005
308.15	16.70	-0.02	298.14	6.556	0.003
308.15	16.72	-0.01	298.14	6.550	-0.003

303.13	10.59	-0.01
303.13	10.59	-0.01
303.14	10.60	-0.01
308.14	16.81	-0.02
308.14	16.83	0.00
308.14	16.82	-0.01
β-Crystalline phase		
278.28	0.597	0.007
278.28	0.607	0.011
278.29	0.610	0.013
283.12	1.090	-0.005
283.13	1.100	0.004
283.13	1.093	-0.003
288.14	2.021	0.009
288.14	2.010	-0.002
288.15	2.010	-0.004
293.14	3.627	0.016
293.14	3.615	0.004
293.14	3.596	-0.015
298.14	6.340	-0.014
298.14	6.361	0.008
298.14	6.351	-0.003

[a] Standard uncertainty u is $u(T) = 0.02$ K and the combined expanded uncertainty U_c (0.95 level of confidence, $k = 2$) is $U_c(p/\mathrm{Pa}) = 0.005\,p/\mathrm{Pa} + 0.05$, except for β-crystalline phase, for which the sublimation pressures are estimated to have a higher uncertainty described as $U_c(p / \mathrm{Pa}) = 0.01\ p / \mathrm{Pa} + 0.1$.

[b] Values are reported with one digit more than is justified by the experimental uncertainty to avoid round-off errors in calculations based on these results.

[c] $\Delta p/\mathrm{Pa} = (p - p_{calc})/\mathrm{Pa}$, where p_{calc} is calculated from the SimCor results (Section 3.6).

[d] Vapour pressures were measured for a mixture of the liquid and α phases. Values were not considered in the SimCor procedure (Section 3.6), but only compared to the correlation derived from other experimental data.

Table 8

Experimental vapour pressures measured using STAT8 apparatus. [a]

T / K	p / Pa [b]	Δp/Pa [c]	T / K	p / Pa [b]	Δp/Pa [c]
L-menthol			DL-menthol		
α-Crystalline + liquid phase [d]			*α-Crystalline phase*		
277.38	0.399	0.018	277.57	0.442	0.002
277.41	0.401	0.018	277.59	0.442	0.001
277.50	0.403	0.016	277.60	0.440	-0.002
282.34	0.758	0.031	282.56	0.853	0.004
282.34	0.756	0.029	282.57	0.852	0.002
282.34	0.759	0.032	282.59	0.854	0.002
286.97	1.352	0.050	287.34	1.562	0.003
286.97	1.354	0.052	287.43	1.579	0.002
286.98	1.355	0.051	287.59	1.607	-0.002
291.56	2.353	0.076	292.79	3.041	-0.001
291.57	2.354	0.075	292.84	3.054	-0.006
291.60	2.364	0.076	292.90	3.078	-0.004

296.23	4.057	0.112	298.16	5.731	-0.001
296.23	4.052	0.107	298.17	5.739	0.001
296.25	4.063	0.109	298.18	5.738	-0.007
300.84	6.809	0.139	303.17	10.13	-0.01
300.85	6.831	0.154	303.19	10.17	0.01
300.86	6.832	0.147	303.20	10.19	0.02
305.45	11.28	0.183	*Liquid phase*		
305.45	11.28	0.191	293.54	4.140	0.009
305.45	11.28	0.184	293.54	4.147	0.016
310.04	18.33	0.22	293.55	4.144	0.008
310.07	18.40	0.23	298.45	6.763	0.008
310.07	18.42	0.24	298.46	6.780	0.018
314.67	29.49	0.22	298.47	6.777	0.008
314.67	29.46	0.20	303.42	10.89	0.00
314.67	29.49	0.23	303.42	10.91	0.02
Liquid phase			303.43	10.91	0.01
303.00	10.38	-0.01	308.42	17.28	0.02
303.00	10.37	-0.02	308.43	17.28	0.01
303.00	10.38	-0.01	308.43	17.29	0.02
308.18	16.76	-0.01	313.42	26.80	-0.04
308.19	16.78	-0.01	313.43	26.82	-0.04
308.20	16.78	-0.02	313.44	26.86	-0.03
313.38	26.57	-0.01	318.39	40.89	0.00
313.38	26.58	0.00	318.40	40.92	-0.01
313.38	26.56	-0.02	318.42	41.00	0.01
318.43	40.80	0.00	323.41	61.49	-0.01
318.46	40.88	-0.02	323.41	61.46	-0.04
318.47	40.94	0.00	323.41	61.46	-0.04
323.48	61.46	-0.06	328.42	90.76	-0.12
323.50	61.58	-0.04	328.42	90.86	-0.02
323.51	61.64	-0.03	328.43	90.86	-0.09
328.56	91.37	-0.06	333.43	132.19	-0.01
328.56	91.37	-0.06	333.44	132.30	0.00
328.56	91.38	-0.05	333.44	132.26	-0.04
332.75	125.19	-0.03	338.35	188.02	-0.18
332.75	125.17	-0.05	338.35	187.96	-0.24
332.75	125.23	0.01	338.36	188.00	-0.33
337.81	180.38	-0.12	343.20	262.65	-0.28
337.81	180.36	-0.14	343.21	262.79	-0.32
337.82	180.51	-0.12	343.21	262.85	-0.26
342.89	256.25	-0.45	348.10	363.80	0.07
342.89	256.28	-0.42	348.11	363.84	-0.12
342.89	256.31	-0.39	348.11	363.84	-0.12
347.88	357.33	-0.43	353.02	497.60	0.26
347.88	357.29	-0.47	353.02	497.73	0.39
347.88	357.26	-0.50	353.03	497.91	0.26
352.88	491.39	-1.00	357.96	673.03	0.64
352.88	491.41	-0.98	357.96	673.21	0.82
352.89	491.42	-1.27	357.96	673.19	0.80
357.86	666.19	-2.10	362.97	903.12	1.39
357.86	666.21	-2.08	362.98	903.45	1.20
357.87	666.45	-2.24	362.98	903.60	1.35
362.82	891.41	-3.69			
362.82	891.38	-3.72			
362.83	891.49	-4.13			

[a] Standard uncertainty u is $u(T) = 0.01$ K and the combined expanded uncertainty U_c (0.95 level of confidence, $k = 2$) is $U_c(p/\mathrm{Pa}) = 0.01p/\mathrm{Pa} + 0.05$.

[b] Values are reported with one digit more than is justified by the experimental uncertainty to avoid round-off errors in calculations based on these results.

[c] $\Delta p/\mathrm{Pa} = (p - p_{calc})/\mathrm{Pa}$, where p_{calc} is calculated from the SimCor results (Section 3.6).

[d] Vapour pressures were measured for a mixture of the liquid and α phases. Values were not considered in the SimCor procedure (Section 3.6), but only compared to the correlation derived from other experimental data.

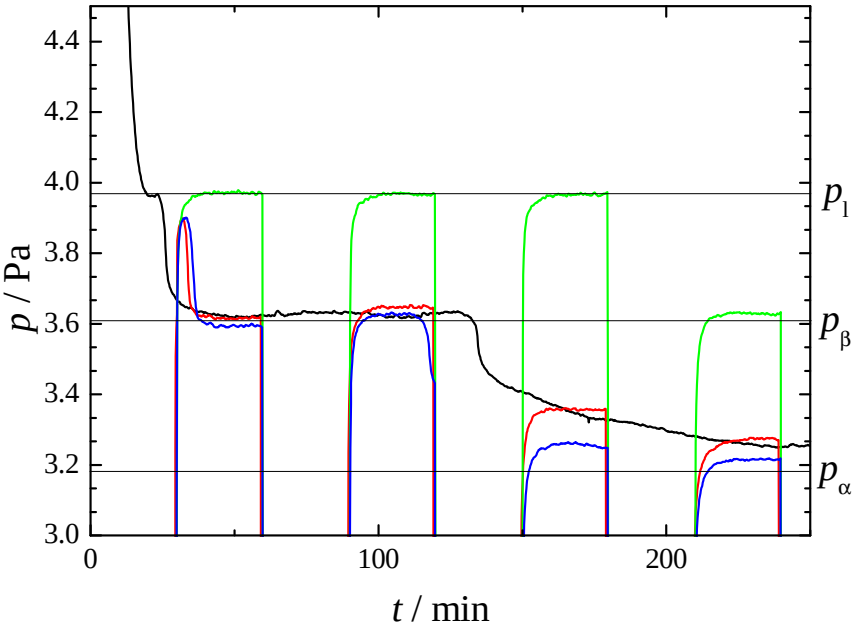

Figure 6. Records from vapour pressure measurement of DL-menthol at 293.15 K.

Liquid sample started to be cooled to 293.15 K at $t = 0$. Records were corrected for the drift. —, liquid remains subcooled for an extended period; —,—, liquid crystalizes to the β phase which starts converting to the α phase after approximately 90 minutes; —, prolonged measuring cycle (three drops in pressure correspond to decrease due to cooling, crystallization to the β form, and transformation to the α form).

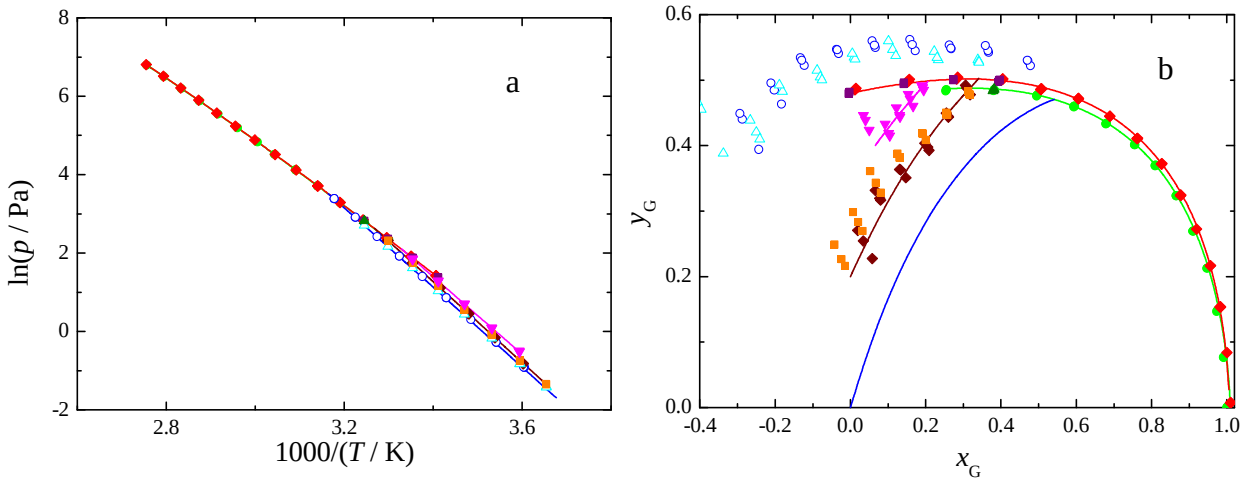

Figure 7. Comparison of vapour pressures of L- and DL-menthol measured in this work. (a) common view; (b) multi-phase arc plot. ●, ▲, L-menthol (liquid, STAT8/STAT6); ◆, ■, DL-menthol (liquid, STAT8/STAT6); ○, △, L-menthol (α crystal + liquid, STAT8/STAT6); ◆, ■, DL-menthol (α crystal, STAT8/STAT6); ▼, DL-menthol (β crystal, STAT6). Lines represent results of SimCor (Section 3.6). Axes x_G and y_G are defined in Section 2 in SD.

3.5 Thermodynamic properties in the ideal-gas state

A menthol molecule consists of a cyclohexane frame with three functional groups (isopropyl, methyl, and hydroxyl) attached to it. A cyclohexane molecule is known to occur in two stable conformations: chair and twist-boat, where the latter is about 5.5 kJ·mol^{-1} less stable [54]. The functional groups can be located either in equatorial or axial positions in both conformations. The menthol molecule adopts a triaxial or triequatorial structure in the chair conformation, in contrast to its diastereomers – iso-, neo-, and neoiso-menthols. The literature studying conformational space of menthol usually assumes the existence of 9 conformers obtained by rotation of asymmetrical tops in the equatorial chair conformation [55]. In some papers, 9 other conformers based on the axial chair conformation are mentioned, but not studied with an argument that they are clearly less stable [56].

The empirical labeling of menthol conformers used in [55, 56] is unclear, and we adopt a notation according to the dihedral angles as used for aliphatic compounds [43]. The designation of each conformer has form "XXX$\varphi\psi$", which starts with its frame conformation ("EQ" for equatorial, "AX" for axial chair, and "TW?" for twist-boat) followed by labels for the dihedral angle of the isopropyl and hydroxyl groups. The question mark in the case of twist-boat stands for the orientation of the twisting axis in the cyclohexane ring; it is substituted by "I" if it passes through the carbon atoms with the isopropyl and methyl group attached, "O" if it passes through the carbon atom with the hydroxyl group attached and one methylene group, and "M" if it passes through two methylene groups. The eight possible cyclohexane frames are schematically displayed in Figure S6 in the SD and characterized in Table 9. Figure 8 highlights dihedral angles φ = 5-4-8-30 and ψ = 4-5-20-31 used in this work to systematically describe the position of the isopropyl and hydroxyl tops, respectively. The minimal dihedral angles are designated as trans (t) ≈ 180°, gauche (g or g') ≈ 60° or -60°, distorted gauche (d or d') ≈ 90° or -90°, narrowed gauche (n or n') ≈ 40° or -40°, and x for an unspecified position. The clockwise (R-) or counterclockwise (S-) rotation of a top from eclipsed position or predominant rotation in the twist-boat frame is marked by using or omitting a prime, respectively.

In total, 57 stable conformers were successfully optimized at the DFT B3LYP-D3/6-311+G(d,p) level of theory. The stable conformers are summarized in Table 9 and listed in Table S4 in the SD. Previous studies [55, 56] expected 9 EQ conformers, but the scan of isopropyl rotation through EQxg conformers in [55] exhibited one additional minimum. It was however considered to be an artifact caused by fixing the hydroxyl group position and was not studied further in [55]. We performed a 2D scan and obtained 10 unambiguous minima, where each belongs to one stable conformer. Our conformational search indeed determined the EQ conformers as the most

stable ones, while all AX and TW conformers possess energies by more than 13 kJ·mol^{-1} greater than the least stable EQ conformer (EQd'g), except for the three AXg'x conformers.

The literature does not reach full agreement about the most stable conformer. Egawa *et al.* [57] detected a mixture of EQ1 conformers (in our notation EQgx) through a combination of gas electron diffraction and calculations at the HF/6-31G(d) level of theory. Avilés Moreno *et al.* [56] stated EQ1int2 (EQgg') was the most stable at the B3LYP/cc-pVDZ level of theory, but EQ1ext (EQgt) at the B3LYP/6-31G(d) level of theory. Schmitz *et al.* [55] determined EQ1ext (EQgt) as the most stable conformer at the three levels of theory: B3LYP/aug-cc-pVTZ, B3LYP/6-311++G(d,p), and MP2/6-311++G(d,p), in agreement with their microwave spectra measurements. Our preliminary calculations without the D3 empirical correction resulted in a relative energy of the EQgg' conformer of only 0.6 kJ mol^{-1} higher than that of EQgt, while B3LYP-D3/6-311+G(d,p) level of theory, which should give more accurate relative energies, predicts the EQgg' and EQgt to be essentially isoenergetic. The LCCSD(T)/aug-cc-pVQZ calculations, however, clearly establish the EQgt conformer as the most stable one. The calculated parameters of the Fourier expansion of three rotating CH_3-tops for the EQgt conformer are given in Table S5 in the SD.

The ideal-gas heat capacities, standard ideal-gas entropies, and ideal-gas thermal enthalpies of enantiopure menthol at p = 0.1 MPa at several temperatures are listed in Table 10 and the calculated dipole moment at 298.15 K is 1.69 D (1 D = 3.335641×10^{-30} C·m). It should be note that including only ten EQ conformers (out of 57) in the calculation of the ideal-gas thermodynamic properties has a negligible impact: $C^0_{p,\mathrm{m}}$ differs by 0.1 % at 300 K and by 1 % at 500 K, and S^0_{m} by 0.1 % at 500 K from the values presented in Table 10 when only ten EQ conformers are considered. No literature data were found for comparison.

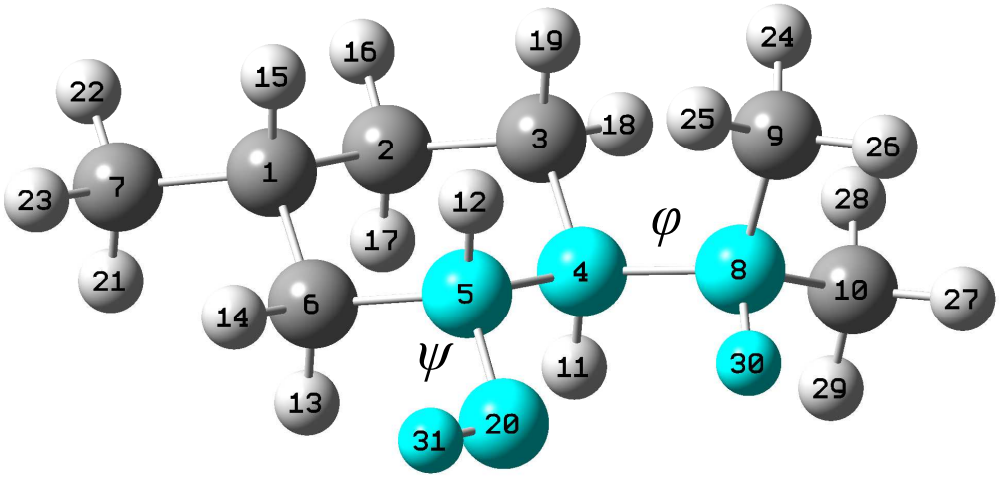

Figure 8. Most stable EQgt conformer of L-menthol with highlighted dihedral angles used to designate the conformation. Numbering of atoms is according to [56] where the conformer is designated as EQ1ext. The dihedral angles φ = 5-4-8-30 (g) and ψ = 4-5-20-31 (t) define the position of the rotating isopropyl and hydroxyl groups.

Table 9

Conformational analysis summary. Stable conformers grouped by the conformation of cyclohexane frame and their range of relative energies.

label	Ring conformation	Twisting atoms	Position of			Number of conformers	ΔE / kJ·mol^{-1} [a]	
			isopropyl	hydroxyl	methyl		min	max
EQ	Chair	-	EQ	EQ	EQ	10	0.0	11.7
AX	Chair	-	AX	AX	AX	9	17.5	33.9
TWI	Twist-boat	1, 4	- [b]	EQ	- [b]	9	26.5	32.0
TWI'	Twist-boat	1, 4	- [b]	AX	- [b]	9	28.4	33.7
TWM	Twist-boat	3, 6	AX	AX	EQ	3	33.7	37.6
TWM'	Twist-boat	3, 6	EQ	EQ	AX	9	31.7	45.0
TWO	Twist-boat	2, 5	EQ	- [b]	AX	5	31.2	35.6
TWO'	Twist-boat	2, 5	AX	- [b]	EQ	3	30.2	32.1

[a] Relative electronic energy calculated at the B3LYP-D3/6-311+G(d,p) level of theory with structure optimization at the same level of theory, except for EQ, for which the energies are calculated at LCCSD(T)/aug-cc-pVQZ with structure optimization at DF-MP2/aug-cc-pVQZ.

[b] Tops connected to atoms at the twisting axis are almost equivalently tilted as the hydrogen atom.

Table 10

Standard molar thermodynamic functions of enantiopure menthol in the ideal gaseous state (in $J \cdot K^{-1} \cdot mol^{-1}$) at p = 0.1 MPa calculated using the R1SM model. [a]

T / K	$C^0_{p,m}$ / $J \cdot K^{-1} \cdot mol^{-1}$	S^0_m / $J \cdot K^{-1} \cdot mol^{-1}$	$(\Delta^T_0 H^0_m / T)$ / $J \cdot K^{-1} \cdot mol^{-1}$
200	159.7	392.8	94.7
210	166.0	400.8	97.9
220	172.4	408.6	101.2
230	178.8	416.4	104.4
240	185.3	424.2	107.7
250	192.0	431.9	110.9
260	198.7	439.5	114.1
270	205.5	447.2	117.4
273.15	207.6	449.6	118.4
280	212.3	454.8	120.7
290	219.3	462.3	123.9
298.15	224.9	468.5	126.6
300	226.2	469.9	127.2
310	233.2	477.4	130.5
320	240.2	484.9	133.9
330	247.1	492.4	137.2
340	254.1	499.9	140.5
350	261.0	507.4	143.9
360	267.9	514.8	147.2
370	274.8	522.3	150.6
380	281.6	529.7	153.9
390	288.3	537.1	157.3
400	295.0	544.5	160.6
500	357.0	617.1	193.9
600	410.0	687.0	225.6
700	454.8	753.7	255.2

[a] Estimated standard uncertainty is 0.005 $C^0_{p,m}$, 0.009 S^0_m, and 0.010 H^0_m.

3.6 Simultaneous treatment of vapour pressures and related thermal data (SimCor method)

The selected experimental vapour data (given in bold in Table 11) were treated simultaneously with $\Delta^g_{cd} C^0_{p,m} = C^0_{p,m}(ig) - C^0_{p,m}(cd)$, where $C^0_{p,m}(ig)$ was from the ideal-gas calculations (Section 3.5) and $C^0_{p,m}(cd)$ was obtained from the condensed-phase data given in Section 3.3 at temperatures below 340 K. Fusion temperatures and enthalpies recommended in this work were

also included in the SimCor calculations. The SimCor method was described in detail in [23] (for the reader's convenience, a detailed description of the SimCor method is also presented in the SD) and was used in our laboratory to develop recommended vapour pressure and thermophysical data for several groups of crystalline and liquid compounds (see, for example, [58] and references therein).

The Clarke and Glew equation [59] with four parameters was used for the SimCor analysis to describe the vapour pressures and the derived thermal properties, which corresponds to a linear temperature dependence of $\Delta_{\mathrm{cd}}^{\mathrm{g}} C_{p,\mathrm{m}}^{0}$. The Clarke and Glew equation has the following form

$$R \ln \frac{p}{p^0} = -\frac{\Delta_{\mathrm{cd}}^{\mathrm{g}} G_{\mathrm{m}}^{0}(\theta)}{\theta} + \Delta_{\mathrm{cd}}^{\mathrm{g}} H_{\mathrm{m}}^{0}(\theta)\left(\frac{1}{\theta} - \frac{1}{T}\right) + \Delta_{\mathrm{cd}}^{\mathrm{g}} C_{p,\mathrm{m}}^{0}(\theta)\left[\frac{\theta}{T} - 1 + \ln\left(\frac{T}{\theta}\right)\right] + \left(\frac{\theta}{2}\right)\frac{\partial \Delta_{\mathrm{cd}}^{\mathrm{g}} C_{p,\mathrm{m}}^{0}}{\partial T}(\theta)\left[\frac{T}{\theta} - \frac{\theta}{T} - 2\ln\left(\frac{T}{\theta}\right)\right] \quad (7)$$

where p^0 = 100 kPa is a reference pressure, θ is a selected reference temperature, R is the molar gas constant, and $\Delta_{\mathrm{cd}}^{\mathrm{g}} G_{\mathrm{m}}^{0}$ and $\Delta_{\mathrm{cd}}^{\mathrm{g}} H_{\mathrm{m}}^{0}$ are the standard molar sublimation/vaporization Gibbs energy and enthalpy, respectively.

The resulting parameters of the Clarke and Glew equation, Eq. (7), together with the standard deviation of the fit, σ, are presented in Table 12. The comparison of the experimental values with the Clarke and Glew equation, Eq. (7), developed using the SimCor method, is shown in Figure 9.

The vapour pressure data for the liquid phase by Guetachew *et al.* [17] agree with our measurements within their experimental uncertainties and were included in the correlation. The sublimation pressures reported in [17] for unspecified polymorph are also in agreement with the

SimCor results for the α form within combined uncertainties, but exhibit a different slope resulting in the sublimation enthalpy deviating by 1.4 kJ·mol^{-1} from the sublimation enthalpy $\Delta_{\alpha}^{\mathrm{g}}H_{\mathrm{m}}^{0}$ obtained by the SimCor method. Kobe *et al.* [14] published a vapour pressure equation without information on enantiomeric excess of menthol and temperature range of the measurement. The experimental method and that they list the normal boiling point indicate that their vapour pressure measurements were performed below atmospheric pressure. The agreement with our correlation for L-menthol is within 3 % above 380 K. At lower temperatures, the deviations increase due to a significantly lower $\Delta_{\mathrm{l}}^{\mathrm{g}}C_{p,\mathrm{m}}^{0}$ resulting from their vapour pressure measurements. The results by Keating *et al.*[15] are not plotted in Figure 9 since they are lower by 15 % to 32 % than the SimCor results in the overlapping temperature range (see the discussion in the next section).

Table 11

Overview of the available experimental vapour pressure data. [a]

Reference	N [b]	$(T_{\mathrm{min}} - T_{\mathrm{max}})$ [c] / K	$(p_{\mathrm{min}} - p_{\mathrm{max}})$/ Pa	Method
		L-Menthol (α-cr)		
Guetachew *et al.* [17]	6	293 – 313	2.9 – 26.5	Static
This work, STAT6	24	274 – 308	0.24 – 15.0	Static
This work, STAT8	27	277 – 315	0.40 – 24.5	Static
		L-Menthol (l)		
Guetachew *et al.* [17] [d]	**11**	**323 – 422**	**61 – 13747**	**Static**
Keating *et al.* [15]	14	298 – 430 / 374 – 404	4.6 – 15000	Chromatography
This work, STAT6	**3**	**308**	**16.7**	**Static**
This work, STAT8	**39**	**303 – 363**	**10.4 – 891**	**Static**
		DL-Menthol (α-cr)		
This work, STAT6	**21**	**274 – 303**	**0.26 – 10.1**	**Static**
This work, STAT8	**18**	**278 – 303**	**0.44 – 10.2**	**Static**
		DL-Menthol (β-cr)		

This work, STAT6	**15**	**278 – 298**	**0.60 – 6.**	**Static**
		DL-Menthol (l)		
Keating *et al.* [15]	21	298 – 500 / 434 - 464	4.5 – 120000	Chromatography
Keating *et al.* [15]	21	298 – 500 / 384 – 414	4.5 – 111000	Chromatography
This work, STAT6	**12**	**293 – 308**	**4.0 – 16.8**	**Static**
This work, STAT8	**45**	**294 – 363**	**4.1 – 904**	**Static**
		Unspecified Menthol (l)		
Kobe *et al.* [14]	S	NA – 490	NA – 101325	Isoteniscope

[a] References reporting single or two vapour pressure points obtained, for example, as part of the synthesis or VLE measurements on multi-component mixtures are not considered.

[b] *N* stands for number of experimental points, S stands for smoothed data.

[c] Temperature range of presented data. If two ranges are listed, they correspond to the range of presented (extrapolated) vapour pressure data and to the range, where the retention times were measured, respectively.

[d] References in bold were included in the SimCor analysis.

Table 12

Parameters of the Clarke and Glew equation, Eq. (7), derived using the SimCor method at the reference temperature θ = 298.15 K and pressure p^0 = 100 kPa.

Compound	$(T_{min} - T_{max})$[a] / K	$\Delta^g_{cd}G^0_m$ / J·mol^{-1}	$\Delta^g_{cd}H^0_m$ / J·mol^{-1}	$\Delta^g_{cd}C^0_{p,m}$ / J·K^{-1}·mol^{-1}	$\frac{\partial \Delta^g_{cd}C^0_{p,m}}{\partial T}$ / J·K^{-2}·mol^{-1}	σ[a] / Pa	σ_r[a]
L-menthol (α crystal)	250 – 316	24590.5 ± 6.4 [b]	84421.4 ± 54.6	-26.436 ± 0.444	-0.2897 ± 0.0171	N/A	N/A
L-menthol (liquid)	303 – 422	23898.4 ± 5.1	72836.6 ± 47.3	-134.27 ± 1.85	-0.4595 ± 0.0526	27	0.66 %
DL-menthol (α crystal)	265 – 306	24214.7 ± 0.8	85596.4 ± 24.1	-19.524 ± 0.440	-0.1385 ± 0.0179	0.007	0.40 %
DL-menthol (β crystal)	270 – 298	23953.7 ± 4.0	82083.7 ± 45.3	-11.306 ± 0.235	0[c]	0.010	0.94 %
DL-menthol (liquid)	293 – 363	23877.4 ± 0.6	72673.5 ± 10.0	-127.14 ± 0.89	-0.7570 ± 0.0350	0.38	0.12 %

[a] The parameters of the Clarke and Glew equation, Eq. (7), developed by the SimCor method are valid over a combined temperature interval of input thermodynamic data.

[a] σ is the standard deviation of the fit defined as $\sigma = \left[\sum_{i=1}^{n} (\Delta p)_i^2 / (n-m)\right]^{1/2}$, where Δp is the difference between the experimental and the smoothed values, n is the number of experimental points used in the fit and m is the number of adjustable parameters of the Clarke and Glew equation, Eq. (7). σ_r is the relative standard deviation of the fit defined as $\sigma_r = \left[\sum_{i=1}^{n} (\Delta \ln p)_i^2 / (n-m)\right]^{1/2}$. Standard deviation for the α crystal of L-menthol (marked as N/A) could not be calculated since no experimental vapour pressure data were included in the correlation.

[b] The uncertainties quoted are standard uncertainty estimations of the optimized parameters. The parameters are reported with more digits than justified by the uncertainties to avoid round-off errors in calculations based on the correlation.

[c] Set as zero due to a short temperature interval and higher uncertainty of the data.

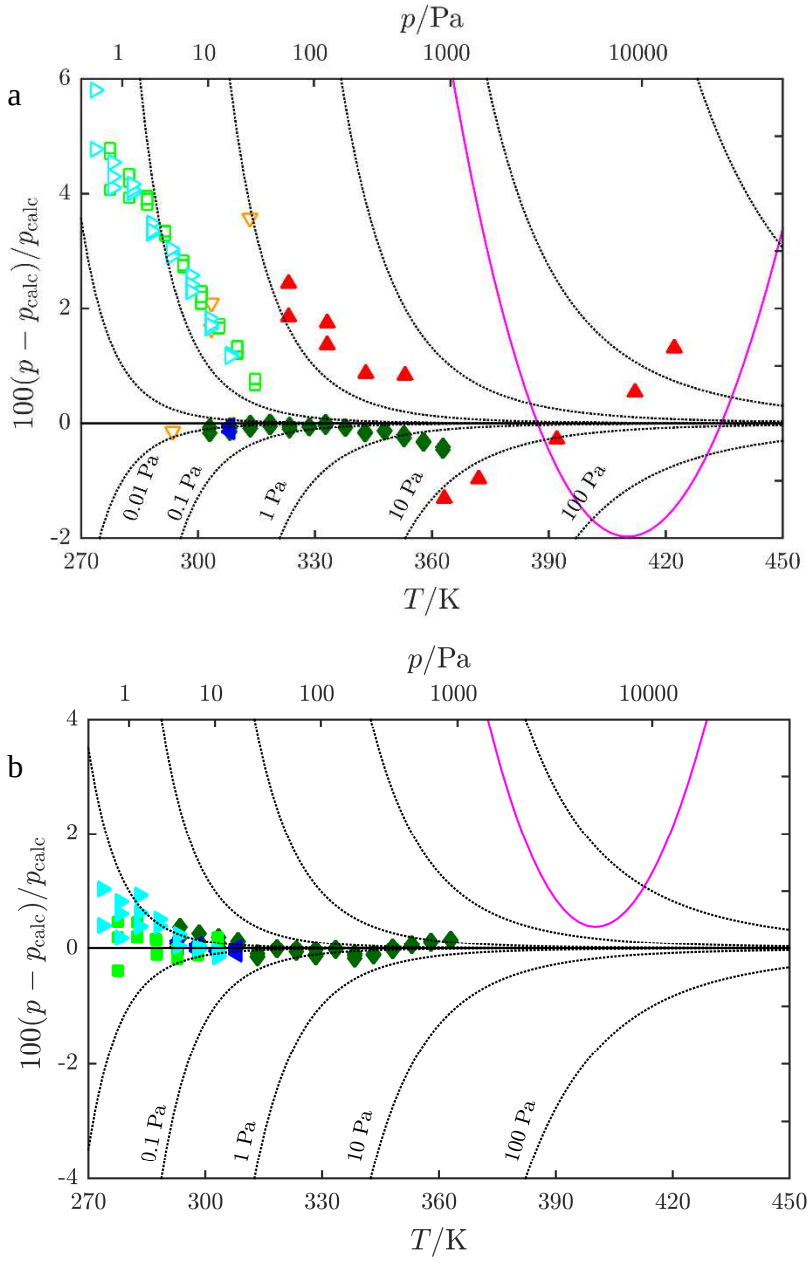

Figure 9. Comparison of experimental vapour pressures p with values p_{calc} developed by the SimCor method for the studied menthols. (a) L-menthol; (b) DL-menthol; ▶,▷, this work

(STAT6, α crystal); ■,□, this work (STAT8, α crystal); ◀, this work (STAT6, liquid); ◆, this work (STAT8, liquid); ▽, Guetachew *et al.* [17] (α crystal); ▲, Guetachew *et al.* [17] (liquid); —, Kobe *et al.* [14]; ▪▪▪▪, lines representing constant absolute deviations. Results by Keating *et al.* [15] are out of scale. Top pressure axis and absolute deviations are plotted for liquid. Empty points were excluded from the SimCor analysis.

3.7 Mutual consistency of the studied thermodynamic properties

Consistency in this work between the fusion parameters measured calorimetrically for DL-menthol and those calculated at the triple point from the vapour pressure measurements, compared in Table 2 is very good. The inconsistencies arising from the long-term coexistence of the liquid and α phase in L-menthol for the vapour pressure, DSC, and adiabatic calorimetry results was already discussed in Section 3.4.

Table 13 summarizes the vaporization/sublimation enthalpy data at 298.15 K. The $\Delta_l^g H_m^0$ values obtained by the SimCor method for L-menthol and DL-menthol at 298.15 K are equal to within their estimated uncertainties, and the consistency with fusion enthalpies supports the SimCor results for $\Delta_\alpha^g H_m^0$. The sublimation enthalpies of unspecified polymorphs of both menthols were previously determined by Chickos *et al.* [47] (via the Clausius-Clapeyron equation from vapour pressures obtained by a head-space method), but they are in disagreement with the SimCor results despite their large stated uncertainty of 5 %. The vaporization enthalpy (and vapour pressure of super cooled liquid in [15]) was determined using indirect gas-liquid chromatography (GLC) method by Hoskovec *et al.* [16] and by Chickos and co-workers [13, 15]. It is outside the scope of this work to analyse the reasons for differences between published values and recommendation of this work (see Table 13); a general analysis of results obtained by the GLC method was recently published by Koutek and co-workers [60, 61]. It is however necessary to mention that results of the GLC method are substantially influenced by i) the choice of reference compounds and quality of their reference vapour pressure data and ii) the length of extrapolation since chromatographic measurements are usually performed well above room temperature, while the results are reported down to 298 K. Hoskovec *et al.* [16] selected *n*-alkanes as reference

compounds, a choice that was recently demonstrated to yield errors of hundreds percent when determining vapour pressures of polar compounds, e.g. 1-alkanols [61]. The resulting 16.2 $kJ \cdot mol^{-1}$ deviation from our value obtained by the SimCor method is therefore not surprising. Chickos and co-workers [13, 15] used 1-alkanols as reference compounds; however extrapolation by at least 75 K was employed, and the reliability of their reference vapour pressures is questionable (see, e.g., disagreement of [62] for 1-hexanol with our recent recommendation [43]). In view of these facts, the agreement of several published values on both vaporization enthalpies and super cooled vapour pressures with the SimCor results is rather good (but it may be fortuitous).

The SimCor results combined with adiabatic calorimetry can be used to derive a recommended value of standard ideal-gas molar entropy S^0_m(ig). The resulting value S^0_m(298.15 K,ig) = (465.3 ± 1.7) $J \cdot K^{-1} \cdot mol^{-1}$ is in agreement with the theoretical value from Table 10 obtained by statistical-thermodynamics calculations, (468.5 ± 4.2) $J \cdot K^{-1} \cdot mol^{-1}$. Figure 10 shows excellent agreement (within 3.5 $J \cdot K^{-1} \cdot mol^{-1}$) between $\Delta^g_{cd} C^0_{p,m}$ obtained from calculated ideal-gas heat capacities and calorimetrically determined heat capacities of crystalline and liquid phases with that derived using the SimCor method, further demonstrating the internal consistency of our vapour pressure and heat capacity data.

Vapour pressures of liquid phase of L-and DL-menthol together with recommended $T_{cr\text{-}l}$ and $\Delta^l_{cr} H^0_m$ from Table 2 were utilized to calculate the differences between the Gibbs energy of the various observed polymorphs and the liquid phase ($\Delta^g_{cr} C^0_{p,m}$ of all crystalline phases were

considered equal to $\Delta_{\alpha}^{g}C_{p,m}^{0}$ since heat capacities were not available for all polymorphs), and the resulting Gibbs-energy diagrams of both menthols are presented in Figure 11.

Table 13

Comparison of vaporization/sublimation enthalpies at 298.15 K

Source	L- or D- menthol (enantiopure)	DL-menthol (racemic)
	$\Delta_{l}^{g}H_{m}^{0}$ / kJ·mol^{-1}	
SimCor, this work	72.8 ± 0.3 [a]	72.7 ± 0.3 [a]
Hoskovec *et al.* [16]	56.6 ± 2.8	
Lipkind and Chickos [13]	72.8 ± 1.9, 75.2 ± 4.3, 76.3 ± 4.4	72.6 ± 2.9
Keating *et al.* [15]	73.7 ± 0.4	74.2 ± 2.8, 73.9 ± 0.4, 73.7 ± 0.4
	$\Delta_{\alpha}^{g}H_{m}^{0}$ / kJ·mol^{-1}	
SimCor, this work	84.4 ± 0.5 [a]	85.6 ± 0.5 [a]
Chickos *et al.* [47]	95.8	78.7

[a] Expanded uncertainties with 0.95 level of confidence were estimated for the SimCor results based on standard error estimations of the parameters and experimental uncertainty of the input data using the error propagation law approximated by the Kragten algorithm [63].

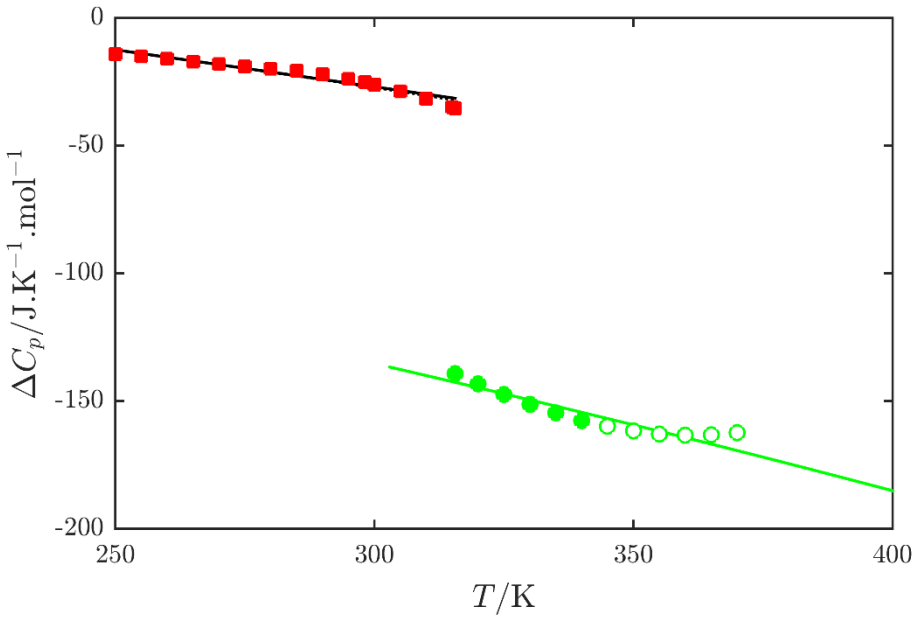

312

313 **Figure 10.** Description of differences in the heat capacity for L-menthol computed by the SimCor

314 method. Combination of adiabatic calorimetry and theoretical calculations: ■, $\Delta_{\alpha}^{\mathrm{g}}C_{p,\mathrm{m}}^{0}$; ●, $\Delta_{\mathrm{l}}^{\mathrm{g}}C_{p,\mathrm{m}}^{0}$; ○,

315 $\Delta_{\mathrm{l}}^{\mathrm{g}}C_{p,\mathrm{m}}^{0}$ (points excluded due to increasing *pVT* correction). SimCor results: ━, $\Delta_{\alpha}^{\mathrm{g}}C_{p,\mathrm{m}}^{0}$; ━, $\Delta_{\mathrm{l}}^{\mathrm{g}}C_{p,\mathrm{m}}^{0}$.

316

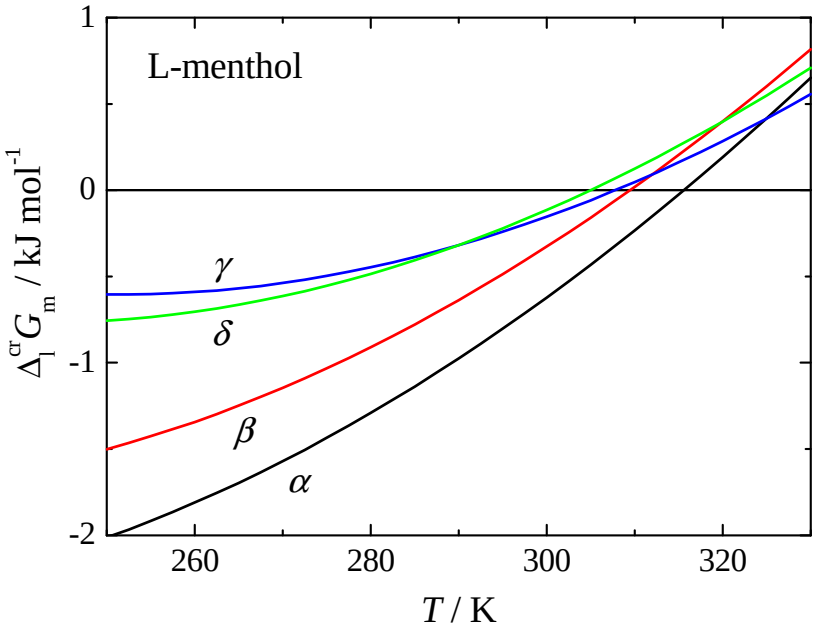

317

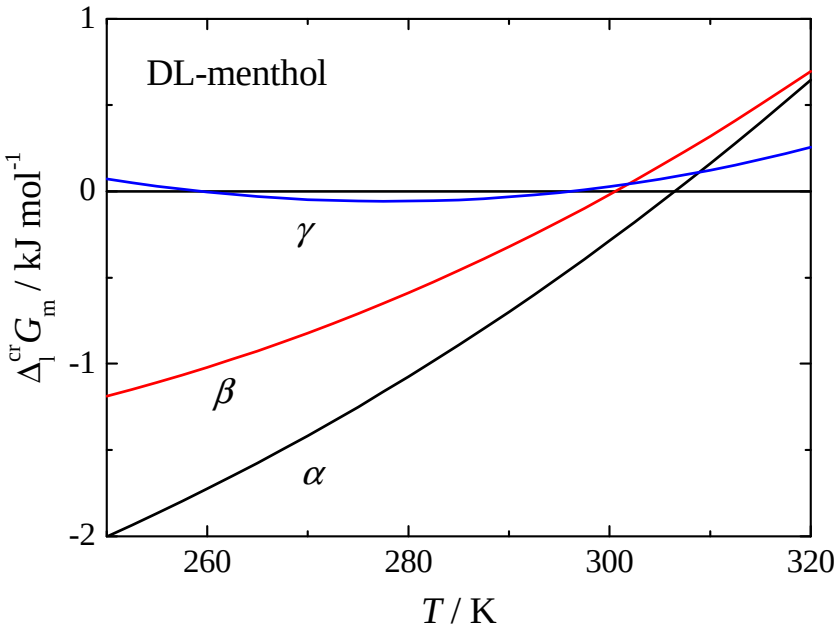

318

319 **Figure 11.** Difference between the Gibbs energy of observed polymorphs and liquid phase $\Delta_l^{cr}G_m$

320 for L- and DL-menthol. —, δ phase; —, γ phase; —, β phase; —, α phase.

321

4 Conclusions

The thermodynamic properties of L- and DL-menthol, including vapour pressures, heat capacity of condensed phases, and phase change temperatures and enthalpies are reported. Many of these are reported for the first time. For both compounds, several concomitant polymorphs were observed during the phase behaviour studies. The kinetics of phase transformation of the β form of DL-menthol to the stable α polymorph and the crystallization of the α polymorph was thoroughly investigated by VT-XRPD. An optimal temperature interval for the formation of the α polymorph was determined based on these experiments. A significantly lower rate of formation of the α polymorph by crystallization compared to that by the β- to α-polymorph transformation was observed (a long-term coexistence of the α polymorph with the liquid phase was detected by VT-XRPD). Experimental thermodynamic data were supplemented by ideal-gas thermodynamic properties obtained by combining statistical thermodynamics and quantum chemical calculations. A thorough conformational analysis performed using the DFT and LCCSD methods revealed the existence of 57 stable conformers, many of which are reported for the first time. Calculated ideal-gas heat capacities were combined with the experimental data on condensed-phase heat capacity, vapour pressure, and phase-change properties and were treated simultaneously to obtain a consistent thermodynamic description. The thermodynamic data and information on polymorphic behaviour reported in this work form a necessary basis for phase equilibrium studies on mixtures containing menthol and should be of interest to a wide range of applications including phase separation processes and environmental modelling.

5 Acknowledgements

Authors V.S., M.F., and K.R. acknowledge financial support from the Czech Science Foundation (GACR No. 17-03875S). Author J.R. acknowledges financial support for the X-ray experimental equipment from the project ASTRA of the Operation program Prague Competitiveness, (Project No. CZ.2.16/3.1.00/24510). The authors would like to acknowledge T.L. Yurkshtovich (Belarusian State University) for specific-rotation measurements on natural L-menthol, H. Kolosovskaya (BelHard Group JSC) for GC-MS analysis of natural L-menthol, and A.F. Kazakov (NIST) for performing calculations at the LCCSD(T)/aug-cc-pVQZ level of theory and for the discussion concerning the statistical-thermodynamics calculations.

This article is a partial contribution of the National Institute of Standards and Technology (NIST) and is not subject to copyright in the United States for the author A.B. Trade names are provided only to specify procedures adequately and do not imply endorsement by the National Institute of Standards and Technology. Similar products by other manufacturers may be found to work as well or better.

Appendix A. Supplementary Data

Supplementary data associated with this article can be found, in the online version, at

Supplementary data contain detailed description of the SimCor method; description of multi-phase Arc plot; tables and figures with details on adiabatic calorimetry experiments and XRPD measurements; figure with labelling of possible cyclohexane frames; list of stable conformers of menthol with their parameters; and parameters of methyl rotations of the most stable EQgt conformer of L-menthol.

References

[1] N. Galeotti, L. Di Cesare Mannelli, G. Mazzanti, A. Bartolini, C. Ghelardini, Menthol: a natural analgesic compound, Neurosci. Lett., 322 (2002) 145-148.

[2] Y. Corvis, P. Negrier, S. Massip, J.-M. Leger, P. Espeau, Insights into the crystal structure, polymorphism and thermal behaviour of menthol optical isomers and racemates, CrystEngComm, 14 (2012) 7055-7064.

[3] M. Okuniewski, K. Paduszyński, U. Domańska, (Solid + liquid) equilibrium phase diagrams in binary mixtures containing terpenes: New experimental data and analysis of several modelling strategies with modified UNIFAC (Dortmund) and PC-SAFT equation of state, Fluid Phase Equilib., 422 (2016) 66-77.

[4] T. Phaechamud, S. Tuntarawongsa, P. Charoensuksai, Evapouration Behaviour and Characterization of Eutectic Solvent and Ibuprofen Eutectic Solution, AAPS PharmSciTech, 17 (2016) 1213-1220.

[5] I. Albuquerque, M. Mazzotti, Influence of Liquid-Liquid Phase Separation on the Crystallization of L-Menthol from Water, Chem. Eng. Technol., 40 (2017) 1339-1346.

[6] Y. Corvis, P. Espeau, Interpretation of the global heat of melting in eutectic binary systems, Thermochim. Acta, 664 (2018) 91-99.

[7] R. Verma, T. Banerjee, Liquid–Liquid Extraction of Lower Alcohols Using Menthol-Based Hydrophobic Deep Eutectic Solvent: Experiments and COSMO-SAC Predictions, Ind. Eng. Chem. Res., 57 (2018) 3371-3381.

[8] F.E. Wright, The Crystallization Of Menthol, J. Am. Chem. Soc., 39 (1917) 1515-1524.

[9] J. Bernstein, R.J. Davey, J.O. Henck, Concomitant Polymorphs, Angew. Chem. Int. Ed. Engl., 38 (1999) 3440-3461.

[10] Y. Corvis, A. Wurm, C. Schick, P. Espeau, New menthol polymorphs identified by flash scanning calorimetry, CrystEngComm, 17 (2015) 5357-5359.

[11] M. Kuhnert-Brandstätter, R. Ulmer, L. Langhammer, Thermoanalytische Untersuchungen an Mentholen 1. Mitteilung, Arch. Pharm., 307 (1974) 497-503.

[12] P. Bombicz, J. Buschmann, P. Luger, N.X. Dung, C.B. Nam, Crystal structure of (1R,2S,5R)-2-isopropyl-5-methyl-cyclohexanol, (−)-menthol, Z. Kristallogr. Cryst. Mater., 214 (1999) 420.

[13] D. Lipkind, J.S. Chickos, An Examination of Factors Influencing the Thermodynamics of Correlation-Gas Chromatography as Applied to Large Molecules and Chiral Separations, J. Chem. Eng. Data, 55 (2010) 698-707.

[14] K.A. Kobe, T.S. Okabe, M.T. Ramstad, P.M. Huemmer, *p*-Cymene Studies. VI. Vapour Pressure of *p*-Cymene, Some of its Derivatives and Related Compounds, J. Am. Chem. Soc., 63 (1941) 3251-3252.

[15] L. Keating, H.H. Harris, J.S. Chickos, Vapour pressures and vaporization enthalpy of (−) α-bisabolol and (dl) menthol by correlation gas chromatography, J. Chem. Thermodyn., 107 (2017) 18-25.

[16] M. Hoskovec, D. Grygarová, J. Cvačka, L. Streinz, J. Zima, S.P. Verevkin, B. Koutek, Determining the vapour pressures of plant volatiles from gas chromatographic retention data, J. Chromatogr. A, 1083 (2005) 161-172.

[17] T. Guetachew, I. Mokbel, I. Batiu, Z. Cisse, J. Jose, Vapour pressures and sublimation pressures of eight constituents of essential oils at pressures in the range from 0.3 Pa to 83.000 Pa, ELDATA: Int. Electron. J. Phys.-Chem. Data, 5 (1999) 43-53.

[18] V. Štejfa, M. Fulem, K. Růžička, C. Červinka, M.A.A. Rocha, L.M.N.B.F. Santos, B. Schröder, Thermodynamic study of selected monoterpenes, J. Chem. Thermodyn., 60 (2013) 117-125.
[19] V. Štejfa, M. Fulem, K. Růžička, C. Červinka, Thermodynamic study of selected monoterpenes II, J. Chem. Thermodyn., 79 (2014) 272-279.
[20] V. Štejfa, M. Fulem, K. Růžička, C. Červinka, Thermodynamic study of selected monoterpenes III, J. Chem. Thermodyn., 79 (2014) 280-289.
[21] V. Štejfa, F. Dergal, I. Mokbel, M. Fulem, J. Jose, K. Růžička, Vapour pressures and thermophysical properties of selected monoterpenoids, Fluid Phase Equilib., 406 (2015) 124-133.
[22] D. Zaitsau, E. Paulechka, D.S. Firaha, A.V. Blokhin, G.J. Kabo, A. Bazyleva, A.G. Kabo, M.A. Varfolomeev, V.M. Sevruk, Comprehensive study of the thermodynamic properties for 2-methyl-3-buten-2-ol, J. Chem. Thermodyn., 91 (2015) 459-473.
[23] K. Růžička, V. Majer, Simultaneous Treatment of Vapour Pressures and Related Thermal Data Between the Triple and Normal Boiling Temperatures for *n*-Alkanes C_5-C_{20}, J. Phys. Chem. Ref. Data, 23 (1994) 1-39.
[24] J. Meija, B. Coplen Tyler, M. Berglund, A. Brand Willi, P. De Bièvre, M. Gröning, E. Holden Norman, J. Irrgeher, D. Loss Robert, T. Walczyk, T. Prohaska, Atomic weights of the elements 2013 (IUPAC Technical Report), in: Pure Appl. Chem., 2016, pp. 265.
[25] R. Sabbah, A. Xu-wu, J.S. Chickos, M.L.P. Leitão, M.V. Roux, L.A. Torres, Reference materials for calorimetry and differential thermal analysis, Thermochim. Acta, 331 (1999) 93-204.
[26] H. Rietveld, A profile refinement method for nuclear and magnetic structures, J. Appl. Crystallogr., 2 (1969) 65-71.
[27] N.V.Y. Scarlett, I.C. Madsen, Quantification of phases with partial or no known crystal structures, Powder Diffr., 21 (2012) 278-284.
[28] G.J. Kabo, A.A. Kozyro, A.P. Marchand, V.V. Diky, V.V. Simirsky, L.S. Ivashkevich, A.P. Krasulin, V.M. Sevruk, M.L. Frenkel, Thermodynamic properties of heptacyclotetradecane C14H16, J. Chem. Thermodyn., 26 (1994) 129-142.
[29] F. Pavese, V.M. Malishev, Routine measurements of specific-heat capacity and thermal-conductivity of high-T_c superconducting materials in the range 4-300 K using modular equipment, in: R.P. Reed, F.R. Fickett, L.T. Summers, M. Stieg (Eds.), Advances in Cryogenic Engineering, Vol 40, Pts A and B: Materials, Plenum Press Div Plenum Publishing Corp, New York, 1994, pp. 119-124.
[30] A.B. Bazyleva, A.V. Blokhin, G.J. Kabo, A.G. Kabo, Y.U. Paulechka, Thermodynamic properties of 1-bromoadamantane in the condensed state and molecular disorder in its crystals, J. Chem. Thermodyn., 37 (2005) 643-657.
[31] A.V. Blokhin, Y.U. Paulechka, G.J. Kabo, Thermodynamic Properties of [C6mim][NTf2] in the Condensed State, J. Chem. Eng. Data, 51 (2006) 1377-1388.
[32] G.W.H. Höhne, W.F. Hemminger, H.-J. Flammersheim, Differential Scanning Calorimetry, 2 ed., Springer Verlag, Berlin, 2003.
[33] M. Fulem, K. Růžička, P. Morávek, J. Pangrác, E. Hulicius, B. Kozyrkin, V. Shatunov, Vapour Pressure of Selected Organic Iodides, J. Chem. Eng. Data, 55 (2010) 4780-4784.
[34] V. Štejfa, M. Fulem, K. Růžička, P. Morávek, New Static Apparatus for Vapour Pressure Measurements: Reconciled Thermophysical Data for Benzophenone, J. Chem. Eng. Data, 61 (2016) 3627-3639.

[35] K. Růžička, M. Fulem, V. Růžička, Recommended Vapour Pressure of Solid Naphthalene, J. Chem. Eng. Data, 50 (2005) 1956-1970.
[36] M. Fulem, K. Růžička, C. Červinka, M.A.A. Rocha, L.M.N.B.F. Santos, R.F. Berg, Recommended vapour pressure and thermophysical data for ferrocene, J. Chem. Thermodyn., 57 (2013) 530-540.
[37] M.J. Frisch, G.W. Trucks, H.B. Schlegel, G.E. Scuseria, M.A. Robb, J.R. Cheeseman, G. Scalmani, V. Barone, B. Mennucci, G.A. Petersson, H. Nakatsuji, M. Caricato, X. Li, H.P. Hratchian, A.F. Izmaylov, J. Bloino, G. Zheng, J.L. Sonnenberg, M. Hada, M. Ehara, K. Toyota, R. Fukuda, J. Hasegawa, M. Ishida, T. Nakajima, Y. Honda, O. Kitao, H. Nakai, T. Vreven, J.A.M. Jr., J.E. Peralta, F. Ogliaro, M. Bearpark, J.J. Heyd, E. Brothers, K.N. Kudin, V.N. Staroverov, T. Keith, R. Kobayashi, J. Normand, K. Raghavachari, A. Rendell, J.C. Burant, S.S. Iyengar, J. Tomasi, M. Cossi, N. Rega, J.M. Millam, M. Klene, J.E. Knox, J.B. Cross, V. Bakken, C. Adamo, J. Jaramillo, R. Gomperts, R.E. Stratmann, O. Yazyev, A.J. Austin, R. Cammi, C. Pomelli, J.W. Ochterski, R.L. Martin, K. Morokuma, V.G. Zakrzewski, G.A. Voth, P. Salvador, J.J. Dannenberg, S. Dapprich, A.D. Daniels, O. Farkas, J.B. Foresman, J.V. Ortiz, J. Cioslowski, D.J. Fox, Gaussian 09, Revision D.01, Gaussian, Inc., Wallingford CT, 2013.
[38] M. Kállay, Z. Rolik, J. Csontos, P. Nagy, G. Samu, D. Mester, J. Csóka, B. Szabó, I. Ladjánszki, L. Szegedy, B. Ladóczki, K. Petrov, M. Farkas, P.D. Mezei, B. Hégely, Mrcc, a quantum chemical program suite, 2017.
[39] R.M. Parrish, L.A. Burns, D.G.A. Smith, A.C. Simmonett, A.E. DePrince, E.G. Hohenstein, U. Bozkaya, A.Y. Sokolov, R. Di Remigio, R.M. Richard, J.F. Gonthier, A.M. James, H.R. McAlexander, A. Kumar, M. Saitow, X. Wang, B.P. Pritchard, P. Verma, H.F. Schaefer, K. Patkowski, R.A. King, E.F. Valeev, F.A. Evangelista, J.M. Turney, T.D. Crawford, C.D. Sherrill, Psi4 1.1: An Open-Source Electronic Structure Program Emphasizing Automation, Advanced Libraries, and Interoperability, J. Chem. Theory Comput., 13 (2017) 3185-3197.
[40] P.R. Nagy, M. Kállay, Optimization of the linear-scaling local natural orbital CCSD(T) method: Redundancy-free triples correction using Laplace transform, J. Chem. Phys., 146 (2017) 214106.
[41] J. Pfaendtner, X. Yu, L.J. Broadbelt, The 1-D hindered rotor approximation, Theor. Chem. Acc., 118 (2007) 881-898.
[42] M.L. Frenkel, G.J. Kabo, K.N. Marsh, G.N. Roganov, R.C. Wilhoit, Thermodynamics of Organic Compounds in the Gas State, Thermodynamics Research Center, College Station, Texas, 1994.
[43] V. Štejfa, M. Fulem, K. Růžička, P. Matějka, Vapour pressures and thermophysical properties of selected hexenols and recommended vapour pressure for hexan-1-ol, Fluid Phase Equilib., 402 (2015) 18-29.
[44] V. Pokorný, V. Štejfa, M. Fulem, C. Červinka, K. Růžička, Vapour Pressures and Thermophysical Properties of Dimethyl Carbonate, Diethyl Carbonate, and Dipropyl Carbonate, J. Chem. Eng. Data, 62 (2017) 3206-3215.
[45] K.S. Pitzer, W.D. Gwinn, Energy Levels and Thermodynamic Functions for Molecules with Internal Rotation I. Rigid Frame with Attached Tops, J. Chem. Phys., 10 (1942) 428-440.
[46] C.C. Marston, G.G. Balint-Kurti, The Fourier grid Hamiltonian method for bound state eigenvalues and eigenfunctions, J. Chem. Phys., 91 (1989) 3571-3576.
[47] J.S. Chickos, D.L. Garin, M. Hitt, G. Schilling, Some solid state properties of enantiomers and their racemates, Tetrahedron, 37 (1981) 2255-2259.

[48] L. Bruner, Ueber die Schmelzwärmen einiger organischen Verbindungen, Ber. Dtsch. Chem. Ges., 27 (1894) 2102-2107.
[49] A.H. White, W.S. Bishop, Dielectric Evidence of Molecular Rotation in the Crystals of Certain Non-aromatic Compounds, J. Am. Chem. Soc., 62 (1940) 8-16.
[50] G.A. Hulett, Continuous change from solid to liquid, Zeit. physikal. Chem., 28 (1899) 629-672.
[51] M. Avrami, Kinetics of Phase Change. II Transformation-Time Relations for Random Distribution of Nuclei, J. Chem. Phys., 8 (1940) 212-224.
[52] V. Štejfa, Development of experimental and theoretical tools for thermodynamic studies in single component systems, Ph.D. Thesis, Department of Physical Chemistry, University of Chemistry and Technology, Prague, 2017, pp. 159.
[53] M. Čenský, V. Roháč, K. Růžička, M. Fulem, K. Aim, Vapour pressure of selected aliphatic alcohols by ebulliometry. Part 1, Fluid Phase Equilib., 298 (2010) 192-198.
[54] D.J. Nelson, C.N. Brammer, Toward Consistent Terminology for Cyclohexane Conformers in Introductory Organic Chemistry, J. Chem. Educ., 88 (2011) 292-294.
[55] D. Schmitz, V.A. Shubert, T. Betz, M. Schnell, Exploring the conformational landscape of menthol, menthone, and isomenthone: a microwave study, Front. Chem., 3 (2015) 1-13.
[56] J.R. Avilés Moreno, F. Partal Ureña, J.J. López González, Hydrogen bonding network in a chiral alcohol: (1R,2S,5R)-(−)-menthol. Conformational preference studied by IR–Raman–VCD spectroscopies and quantum chemical calculations, Struct. Chem., 24 (2013) 671-680.
[57] T. Egawa, M. Sakamoto, H. Takeuchi, S. Konaka, Structural Determination of Menthol and Isomenthol, a Minty Compound and Its Nonminty Isomer, by Means of Gas Electron Diffraction Augmented by Theoretical Calculations, J. Phys. Chem. A, 107 (2003) 2757-2762.
[58] K. Růžička, M. Fulem, T. Mahnel, C. Červinka, Recommended vapour pressures for aniline, nitromethane, 2-aminoethanol, and 1-methyl-2-pyrrolidone, Fluid Phase Equilib., 406 (2015) 34-46.
[59] E.C.W. Clarke, D.N. Glew, Evaluation of thermodynamic functions from equilibrium constants, Trans. Faraday Soc., 62 (1966) 539-547.
[60] K. Růžička, B. Koutek, M. Fulem, M. Hoskovec, Indirect Determination of Vapour Pressures by Capillary Gas–Liquid Chromatography: Analysis of the Reference Vapour-Pressure Data and Their Treatment, J. Chem. Eng. Data, 57 (2012) 1349-1368.
[61] B. Koutek, T. Mahnel, P. Šimáček, M. Fulem, K. Růžička, Extracting Vapour Pressure Data from GLC Retention Times. Part 1: Analysis of Single Reference Approach, J. Chem. Eng. Data, 62 (2017) 3542-3550.
[62] J. N'Guimbi, H. Kasehgari, I. Mokbel, J. Jose, Tensions de vapeur d'alcools primaires dans le domaine 0,3 Pa à 1,5 kPa, Thermochim. Acta, 196 (1992) 367-377.
[63] J. Kragten, Tutorial review. Calculating standard deviations and confidence intervals with a universally applicable spreadsheet technique, Analyst, 119 (1994) 2161-2165.